

ELECTRONIC SUPPLEMENTARY INFORMATION

**Cyclic Metal(oid) Clusters Control Platinum-Catalysed
Hydrosilylation Reactions: From Soluble to Zeolite and MOF
Catalysts**

Miguel Rivero-Crespo,^{a,b*} Judit Oliver-Meseguer,^a Klaudia Kapłońska,^c Piotr Kuśtrowski,^c Emilio Pardo,^d José Pedro Cerón-Carrasco^{e*} and Antonio Leyva-Pérez.^{a*}

^a Instituto de Tecnología Química. Universitat Politècnica de València–Consejo Superior de Investigaciones Científicas. Avda. de los Naranjos s/n, 46022, Valencia, Spain.

^b Current address: Department of Chemistry and Applied Biosciences. Swiss Federal Institute of Technology (ETH) Zürich. Vladimir-Prelog-Weg 1-5/10. 8093 Zürich. Switzerland.

^c Faculty of Chemistry, Jagiellonian University. Gronostajowa 2, 30-387 Krakow. Poland.

^d Instituto de Ciencia Molecular (ICMol), Universidad de Valencia, 46980 Paterna, Valencia, Spain.

^e Reconocimiento y Encapsulación Molecular (REM), Universidad Católica de Murcia (UCAM) (Spain).

TABLE OF CONTENTS:

- Experimental section:	S3
o General	S3
o Procedures for the synthesis of Pt catalysts	S3
o Typical reaction procedures	S4
o Synthesis of substituted <i>para</i> -phenyldimethyl silanes	S7
o Compound characterization	S8
o Computational details	S12
- Graphical method	S12
o General discussion	S12
o Simplicity and associated error	S13
o Enthalpy value	S15
o Entropy value	S16
o Hammett parameter	S18
o <i>KIE</i> values	S19
- Hydrosilylation of alkynes. Kinetic experiments	S20
o Tables S1-11	S20
o Figures S1-S16	S28
- Hydrosilylation of alkynes. Reactivity, computational, mechanism	S37
o Table S12	S37
o Figures S16-S26	S38
o Movies S1-S4	S45
- Hydrosilylation of alkenes	S47
o Table S13	S47
o Figures S27-S29	S47
- Dehydrogenative silylation of alcohols	S49
o Figures S30-S31	S49
- References	S50

Experimental Section.

General.

Reagents were obtained from commercial sources and used without further purification unless otherwise indicated. Anhydrous solvents were obtained from a resin-exchanger apparatus. Reactions were performed in conventional round-bottomed flasks or sealed vials equipped with a magnetic stirrer. Most of the products have been previously described in the literature, and they are here characterized by GC-MS, ^1H -, ^{13}C or DEPT, and compared with the existing literature (all references provided with the compound). TLCs and flash chromatography were performed on silica and silica plates, respectively. Gas chromatographic analyses were performed in an instrument equipped with a 25 m capillary column of 5% phenylmethylsilicone. GC/MS analyses were performed on a spectrometer equipped with the same column as the GC and operated under the same conditions. ^1H -, ^{13}C and DEPT were recorded in a 300 MHz instrument using CDCl_3 as solvent unless otherwise indicated, containing TMS as internal standard. The metal content of the solids and filtrates was determined by the inductively coupled plasma-atomic emission spectroscopy (ICP-AES) by disaggregation of the solid in aqueous acid mixture. X-ray photoelectron spectroscopy (XPS) measurements were recorded in a spectrometer using non-monochromatic Mg KR (1253.6 eV) X-ray source working at 50 W, after sticking, without sieving, the solid on a molybdenum plate with scotch tape film, followed by air drying. As an internal reference for the peak positions in the XPS spectra, the C1s peak has been set at 284.5 eV. The Fourier transform infrared (FTIR) using CO as a probe molecule was recorded on a spectrometer equipped with a homemade IR cell able to work at 77 K temperature range. Prior to CO adsorption experiments, the sample was evacuated at 298 K under vacuum (10^{-6} mbar) for 1 h. Deconvolution of the IR spectra has been performed in the Origin software using Gaussian curves where the full width at half-maximum (fwhm) of the individual bands has been taken as constant. The peak areas are normalized to the sample weight. Electron microscopy studies were performed on a Jeol microscope operated at 100-200kV after impregnating a dispersion of the solid sample on a Cu grid and leaving to evaporate for, at least, 4 h.

Procedures for the synthesis of Pt catalysts.

Pt/NaY 1 wt% was prepared by ionic exchange of a NaY zeolite. Typically, 10 g of the corresponding Y zeolite was suspended in 1 L of water and stirred for 12 h at 70 °C. A

0.01 M solution of $\text{Pt}(\text{NH}_3)_4(\text{NO}_3)_2$ was added at the rate of 1.5×10^{-4} mol Pt/h to give a suspension at 70 °C with stirring. After addition of 50 mL (0.197 g of the platinum salt), the suspension was stirred for another 12 h at 70 °C. Subsequently the support was filtered and re-suspended in 1 L of demineralized water at RT to remove nitrates, exchanged cations, and non-exchanged precursor. This procedure (filtered and washing) was repeated twice. After that, the zeolite was re-suspended in 250 mL of acetone at RT, and filtered again, and re-suspended in 250 mL of diethyl ether to improve the dry process. After filtering, the catalyst was calcined at 300 °C for 2 h in an oven under air flow. The Pt loading of the catalysts was determined by the Inductively Coupled Plasma-Atomic Emission Spectroscopy (ICP-AES) technique after disaggregation of the solid in aqueous acid mixture, obtaining a 0.8% of platinum in the zeolite.

Pt₃/NaY 1 wt%:^{S1} Pt/YNa 1 wt% was put into a 50 ml flask equipped with a septum and a balloon. CO (1 atmosphere) was introduced and the flask heated at 80 °C during 20 hours. After that, the flask was evacuated at vacuum and a new portion of CO (1 atmosphere) was added and carbonylation was continued at 115 °C during 50 hours. A pale purple solid was obtained.

PtCl₂/SiO₂ 1 wt% was obtained by incipient wetness impregnation of an aqueous solution of $\text{H}_2\text{PtCl}_6 \cdot x\text{H}_2\text{O}$ over commercial SiO_2 nanopowder followed by 3 hours of drying at 100 °C. The catalyst was calcined at 200 °C in air for 16 hours and then at 300 °C in air for 7 more hours.

Pt₁/MOF^{S2} was obtained after soaking crystals of the parent $\text{MOFNi}_2\text{II}\{\text{NiII}_4[\text{CuII}_2(\text{Me}_3\text{mpba})_2]_3\} \cdot 54\text{H}_2\text{O}$ (51.8 mg, 0.015 mmol) in a $\text{H}_2\text{O}/\text{CH}_3\text{OH}$ (1:1) solution of $[\text{Pt}(\text{NH}_3)_4](\text{NO}_3)_2$ (5.8 mg, 0.015 mmol) for 12 hours. The process was repeated five more times to ensure the total replacement of Ni(II) cations by Pt(II) ones.

Supported Pt₁ catalyst was synthesized following the procedure in ref. 5b from the main text. In order to keep Pt₁ species in solution, Pt Karstedt's catalyst was used in combination with TEMPO in order to avoid reduction-induced aggregation. Pt₃ species were synthesized following the procedures reported in ref. 9-11 from the main text.

Typical reaction procedures.

Typical reaction procedure for the hydrosilylation of alkynes.

Soluble Pt catalysts. A solution of the corresponding alkyne (0.5 mmol) and HSiEt₃ (0.6 mmol) in toluene (1.0 mL) was placed in a vial capped with a septum and magnetically stirred in an oil bath at 110 °C for 5 min. Then, the corresponding amount of Karstedt's catalyst (dissolved in toluene or not) was added to the reaction mixture, together or not with 10 mol% of TEMPO, and aliquots (25 μL) were taken periodically for GC analysis after diluting with dichloromethane (1.0 mL), using *n*-dodecane (0.05 mmol) as an external standard. At the end of the reaction, the solvent was removed through rotary evaporation and the products were purified by flash column chromatography or preparative TLC on silica. Alternatively, 1,1,2,2-tetrachloroethane (0.5 mmol) was added to the crude as internal standard for ¹H-NMR yield quantification and the mixture was dissolved in 1 ml of CDCl₃.

Solid Pt catalysts. A solution of the corresponding alkyne (0.5 mmol) was placed in a vial containing the solid Pt-based catalyst, capped with a septum and magnetically stirred in an oil bath at 110 °C for 5 min. Then, silane (0.6 mmol) was added to the reaction mixture, and aliquots (25 μL) were taken periodically for GC analysis after diluting with dichloromethane (1.0 mL), using *n*-dodecane (0.05 mmol) as an external standard. At the end of the reaction, the solvent was removed through rotary evaporation and the products were purified by flash column chromatography or preparative TLC on silica. Alternatively, 1,1,2,2-tetrachloroethane (0.5 mmol) was added to the crude as internal standard for ¹H-NMR yield quantification and the mixture was dissolved in 1 ml of CDCl₃.

Typical reaction procedure for the hydrosilylation of alkenes.

Soluble Pt catalysts. A solution of the corresponding alkene (0.5 mmol), silane (0.6 mmol) and *n*-dodecane (0.05 mmol, internal standard) in toluene (1.0 mL) was placed in a vial capped with a septum and magnetically stirred in an oil bath at 110 °C for 5 min. Then, the corresponding amount of Pt catalyst dissolved in toluene was added to the reaction mixture, and aliquots (25 μL) were taken periodically for GC analysis after diluting with dichloromethane (1.0 mL). At the end of the reaction, the solvent was removed through rotary evaporation and the products were purified by flash column chromatography or preparative TLC on silica. Alternatively, 1,1,2,2-tetrachloroethane (0.5 mmol) was added to the crude as internal standard for ¹H-NMR yield quantification and the mixture was dissolved in 1 ml of CDCl₃.

Solid Pt catalysts. A solution of the corresponding alkene (0.5 mmol) in toluene (1.0 mL) was placed in a vial containing the solid Pt-based catalyst, capped with a septum and magnetically stirred in an oil bath at 110 °C for 5 min. Then, silane (0.6 mmol) was added to the reaction mixture, and aliquots (25 µL) were taken periodically for GC analysis after diluting with dichloromethane (1.0 mL), using *n*-dodecane (0.05 mmol) as an external standard. At the end of the reaction, the solvent was removed through rotary evaporation and the products were purified by flash column chromatography or preparative TLC on silica. Alternatively, 1,1,2,2-tetrachloroethane (0.5 mmol) was added to the crude as internal standard for ¹H-NMR yield quantification and the mixture was dissolved in 1 ml of CDCl₃.

Typical reaction procedure for the dehydrogenative hydrosilylation of alcohols.

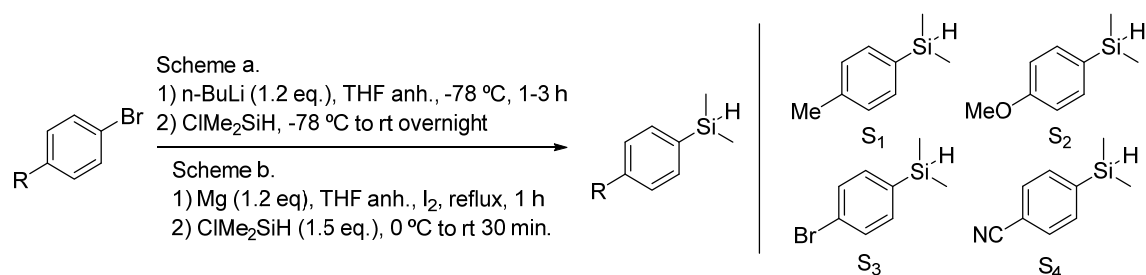
Soluble Pt catalysts. A solution of the corresponding alcohol (0.25 mmol), silane (0.50 mmol) and *n*-dodecane (0.05 mmol, internal standard) in 1,4-dioxane (0.25 mL) was placed in a vial capped with a septum and magnetically stirred in an oil bath at 110 °C for 5 min. Then, the corresponding amount of Pt catalyst dissolved in 1,4-dioxane was added to the reaction mixture, and aliquots (10 µL) were taken periodically for GC analysis after diluting with dichloromethane (1.0 mL). At the end of the reaction, the solvent was removed through rotary evaporation and the products were purified by flash column chromatography or preparative TLC on silica. Alternatively, 1,1,2,2-tetrachloroethane (0.5 mmol) was added to the crude as internal standard for ¹H-NMR yield quantification and the mixture was dissolved in 1 ml of CDCl₃.

Solid Pt catalysts. A solution of the corresponding alcohol (0.25 mmol) in 1,4-dioxane (0.25 mL) was placed in a vial containing the solid Pt-based catalyst, capped with a septum and magnetically stirred in an oil bath at 110 °C for 5 min. Then, silane (0.50 mmol) was added to the reaction mixture, and aliquots (10 µL) were taken periodically for GC analysis after diluting with dichloromethane (1.0 mL), using *n*-dodecane (0.05 mmol) as an external standard. At the end of the reaction, the solvent was removed through rotary evaporation and the products were purified by flash column chromatography or preparative TLC on silica. Alternatively, 1,1,2,2-tetrachloroethane (0.5 mmol) was added to the crude as internal standard for ¹H-NMR yield quantification and the mixture was dissolved in 1 ml of CDCl₃.

Typical reaction procedure to obtain kinetic profiles.

The reactions were carried out following the aforementioned procedures but in larger scale (2 mmol of limiting reagent: alkyne, alkene or alcohol, respectively) inside 10 ml Biotage® microwave reaction vials sealed with a cap with septum (withstand pressures up to 30 bar) and using dodecane (0.5 mmol) as internal standard. After all the reagents were mixed with the solvent inside the vial containing the magnetic stirring bar, the vial was sealed with a cap with septum and heated at the desired temperature for 15 minutes before adding the catalyst. After the addition of the catalyst, aliquots were extracted through the septum with a Hamilton® syringe at the desired times, diluted with ethyl acetate and analysed by GC-FID.

Synthesis of *para*-substituted phenyldimethyl silanes.



(4-methyl)-phenyldimethyl silane (S₁) and (4-bromo)-phenyldimethyl silane (S₃) were prepared following reaction scheme a. 4-Bromotoluene (1.2 g, 7 mmol) was diluted with anhydrous THF (30 mL) into a 100 mL round bottom flask equipped with magnetic stirrer. *n*-BuLi diluted in hexanes (8.4 mmol, 1.2 eq.) was added slowly to the mixture at -78 °C and stirred during 3 h. After this, ClMe₂SiH (0.97 g, 10 mmol) was added to the mixture, taken to room temperature and stirred overnight. The same procedure was followed to obtain S₃ using 1,4-dibromobenzene (3.0 g, 12.7 mmol) and the corresponding amounts of the other reagents. Products were purified by flash chromatography using silica as stationary phase and hexane as eluent.

(4-methoxy)-phenyldimethyl silane (S₂) and (4-cyano)-phenyldimethyl silane (S₄) were prepared following reaction scheme b. 4-Bromoanisole (1.2 mL, 10 mmol) was added to a 100 mL round bottom flask containing 30 ml of anhydrous THF, Mg turnings (290 mg, 12 mmol) and a magnetic stirrer. Two crystals of iodine were added to catalyse the reaction, which was taken to reflux for 1 hour under constant stirring and then placed into an ice bath at 0 °C. ClMe₂SiH (1.69 mL, 18.5 mmol) was added and reaction was stirred

overnight. The same procedure was followed to obtain S4 using 4-bromo benzonitrile (1.84 g, 10 mmol). Products were purified by flash chromatography using silica as stationary phase and hexane as eluent.

Compound characterization.

Triethyl(1-phenylvinyl)silane 8a.^{S3} GC-MS (*m/z*, M^+ 218.2), major peaks found: 218.2 (5%), 189.2 (79%), 161.2 (100%), 133.2 (48%), 107.2 (37%), 87.2 (20%), 59.2 (20%). ¹H NMR (δ , ppm; *J*, Hz): 7.00-7.40 (5H, m), 5.78 (1H, d, *J* = 3.1), 5.48 (1H, d, *J* = 3.1), 0.87 (9H, m), 0.57 (6H, m). ¹³C NMR (δ , ppm; *J*, Hz): 150.5 (C), 145.5 (C), 128.8 (CH₂), 128.1 (2 x CH), 126.7 (2 x CH), 126.1 (CH), 7.3 (3 x CH₃), 3.3 (3 x CH₂). HRMS (ESI) [M^+ , major peak; calculated for C₁₄H₂₂Si: 218.1491] found 218.1496 *m/z*.

Dimethyl(phenyl)(1-phenylvinyl)silane 8b ($\alpha + \beta$). ¹H NMR (δ , ppm; *J*, Hz): 7.58 – 6.97 (m, 27H), 6.86 (d, *J* = 19.1 Hz, 1H), 6.50 (d, *J* = 19.2 Hz, 1H), 5.90 (d, *J* = 2.9 Hz, 1H), 5.58 (d, *J* = 2.9 Hz, 1H), 0.54 – 0.30 (m, 10H). ¹³C NMR (δ , ppm; *J*, Hz): 153.36, 147.64, 146.49, 140.89, 140.59, 140.49, 140.16, 136.36, 136.31, 136.25, 131.44, 131.39, 131.36, 130.84, 130.55, 130.48, 130.42, 130.22, 130.18, 130.15, 130.12, 129.96, 129.43, 129.19, 128.83, 128.79, 128.71, 127.63, 0.00, -0.19.

Phenyl(1-phenylvinyl)silane 8c ($\alpha + \beta$). ¹H NMR (δ , ppm; *J*, Hz): 8.05 – 6.71 (m, 135H), 6.56 (dd, *J* = 19.1, 3.2 Hz, 1H), 6.42 (dt, *J* = 18.9, 3.2 Hz, 2H), 6.15 (d, *J* = 2.5 Hz, 1H), 5.74 (d, *J* = 2.4 Hz, 1H), 4.90 – 4.50 (m, 8H), 2.97 (s, 1H), 2.27 (s, 14H). ¹³C NMR (δ , ppm; *J*, Hz): 148.30, 136.82, 136.71, 134.54, 134.45, 132.21, 131.09, 128.84, 128.78, 128.00, 127.74, 127.61, 127.56, 127.53, 127.46, 127.26, 127.19, 127.07, 126.87, 125.94, 125.68, 125.65, 125.43, 124.27, 118.35, 76.41, 76.12, 75.98, 75.56, 20.42, 0.00.

*Triethyl(1-(*o*-tolyl)vinyl)silane 9*.^{S3} IR (ν , cm⁻¹): 2953, 2876, 1737, 1366, 1217, 729. GC-MS (*m/z*, M^+ 232.2), major peaks found: 232.2 (28%), 203.2 (100%), 175.2 (44%), 147.2 (45%), 115.2 (29%), 87.2 (59%), 59.2 (34%). ¹H NMR (δ , ppm; *J*, Hz): 6.96 (4H, m), 5.60 (2H, q, *J* = 3.4), 2.11 (3H, s), 0.85 (9H, m), 0.54 (6H, m). ¹³C NMR (δ , ppm; *J*, Hz): 150.0 (C), 143.9 (C), 132.8 (C), 128.9 (CH), 127.9 (CH₂), 126.6 (CH), 124.6 (CH), 124.1 (CH), 19.2 (CH₃), 6.2 (3 x CH₃), 1.5 (3 x CH₂). HRMS (ESI) [M^+ , major peak; calculated for C₁₅H₂₄Si: 232.1647] found 232.1651 *m/z*.

(1-(2-Chlorophenyl)vinyl)triethylsilane 10.^{S3} GC-MS (m/z, M⁺• 252.1), major peaks found: 252.1 (<1%), 223.2 (100%), 195.1 (7%), 169.1 (12%), 141.1 (13%), 93.1 (7%), 59.2 (7%). ¹H NMR (δ, ppm; J, Hz): 7.09 (4H, m), 5.68 (2H, dd, J = 8.6, 3.0), 0.85 (9H, m), 0.61 (6H, m). ¹³C NMR (δ, ppm; J, Hz): 149.4 (C), 144.4 (C), 133.0 (C), 131.6 (CH²), 129.7 (CH), 129.3 (CH), 127.0 (CH), 126.2 (CH), 7.2 (CH₃), 3.5 (CH₂).

(1-cyclohexylvinyl)triethylsilane 11a (α + β). ¹H NMR (δ, ppm; J, Hz): 5.98 (dd, J = 18.9, 6.0 Hz, 1H), 5.48 (dd, J = 18.9, 1.5 Hz, 1H), 2.08 – 1.89 (m, 1H), 1.80 – 1.68 (m, 4H), 1.41 – 1.03 (m, 6H), 0.92 (t, J = 7.9 Hz, 9H), 0.54 (q, J = 7.9 Hz, 6H). ¹³C NMR (δ, ppm; J, Hz): 153.31 (CH), 120.95 (CH), 43.21 (CH), 31.52 (2 x CH₂), 25.27 (2 x CH₂), 25.03 (CH₂), 6.35 (3 x CH₃), 2.55 (3 x CH₂).

(1-cyclohexylvinyl)dimethyl(phenyl)silane 11b (α + β). ¹H NMR (δ, ppm; J, Hz): 7.74 – 6.90 (m, 28H), 6.00 (dd, J = 18.7, 5.9 Hz, 2H), 5.78 – 5.52 (m, 3H), 5.32 (d, J = 2.6 Hz, 1H), 1.93 (dt, J = 11.0, 3.1 Hz, 3H), 1.87 – 1.41 (m, 16H), 1.41 – 0.78 (m, 15H), 0.51 – 0.13 (m, 20H). ¹³C NMR (δ, ppm; J, Hz): 158.25, 157.23, 141.90, 141.28, 140.22, 136.38, 136.34, 136.22, 135.42, 132.01, 131.42, 131.18, 131.13, 130.62, 130.28, 130.24, 130.06, 130.02, 127.69, 126.68, 126.28, 79.83, 79.41, 78.98, 46.39, 45.73, 35.93, 34.74, 29.33, 28.68, 28.64, 28.44, 23.83, 2.37, 0.00, -0.02.

Benzyl(1-(3-methoxyphenyl)vinyl)dimethylsilane 12.^{S3} GC-MS (m/z, M⁺• 282.1), major peaks found: 282.1 (40%), 191.2 (100%), 165.2 (63%), 121.2 (10%), 91.2 (11%), 59.2 (7%). ¹H NMR (δ, ppm; J, Hz): 6.81 (9H, m), 5.73 (1H, d, J = 2.8), 5.43 (1H, d, J = 2.8). 3.66 (3H, s), 2.08 (2H, s), 0.0 (6H, s). ¹³C NMR (δ, ppm; J, Hz): 159.4 (C), 151.7 (C), 146.1 (C), 139.6 (C), 129.1 (CH), 128.6 (CH₂), 128.3 (2 x CH), 128.1 (2 x CH), 124.1 (CH), 119.4 (CH), 112.6 (CH), 111.8 (CH), 55.2 (CH₃), 25.6 (CH₂), -2.8 (2 x CH₃).

Dimethyl(phenylethyl)(phenyl)silane 18.^{S4} GC-MS (m/z, M⁺• 240.1), major peaks found: 240.1 (<1%), 225.3 (14%), 197.3 (6%), 163.3 (9%), 162.3 (56%), 136.3 (17%), 135.3 (100%), 121.3 (31%), 105.3 (12%). ¹H NMR (δ, ppm; J, Hz): 7.11 (10H, m), 2.55 (2H, m), 1.04 (2H, m), 0.18 (6H, s).

Benzyl(dimethyl(phenethyl)silane 19.^{S5} GC-MS (m/z, M⁺• 254.1), major peaks found: 254.1 (<1%), 239.2 (1%), 164.2 (15%), 163.2 (93%), 136.2 (13%), 135.2 (100%), 121.2 (14%), 91.2 (14%), 59.2 (36%). ¹H NMR (δ, ppm; J, Hz): 7.13 (10H, m), 2.53 (2H, m), 2.03 (2H, s), 0.81 (2H, m) 0.01 (6H, s).

1,1,1,3,3-Pentamethyl-3-phenethylsiloxane 20.^{S6} ¹H NMR (δ, ppm; J, Hz): 7.11 (5H, m), 2.53 (2H, m), 0.80 (2H, m), 0.01 (9H, s), -0.05 (6H, s).

(4-Methoxyphenethyl)dimethyl(phenyl)silane 21a.^{S7a} GC-MS (m/z, M⁺ 270.1), major peaks found: 270.1 (12%), 255.1 (4%), 227.2 (21%), 192.2 (69%), 167.2 (44%), 135.2 (100%), 122.2 (43%), 105.2 (10%). ¹H NMR (δ, ppm; J, Hz): 7.33 (9H, m), 3.91 (3H, s), 2.76 (2H, m), 1.30 (2H, m), 0.46 (6H, s).

(4-Bromophenethyl)dimethyl(phenyl)silane 21b.^{S7b} ¹H NMR (δ, ppm; J, Hz): 7.43-7.35 (d, J = 8.5, 2H), 7.25-7.17 (m, 3H), 7.07 (t, J = 7.1 Hz, 1H), 7.01-6.99 (m, 3H), 2.54 – 2.48 (m, 2H), 2.10i (s, 2H), 0.86 – 0.80 (m, 2H), -0.01 (s, 6H). ¹³C NMR (δ, ppm; J, Hz): 143.9 (C), 140.0 (C), 131.5 (CH), 129.6 (CH), 128.4 (CH), 128.2 (CH), 124.0 (CH), 119.1 (C), 29.3(CH₂), 25.5(CH₂), 16.7(CH₂), -3.6 (2xCH₃).

1,1,1,3,3-Pentamethyl-3-(3-nitrophenethyl)siloxane 22. ¹H NMR (δ, ppm; J, Hz): 7.48 (4H, m), 2.59 (2H, m), 0.80 (2H, m), 0.01 (9H, s), -0.03 (6H, s).

3-(2-(Dimethyl(phenyl)silyl)ethyl)aniline 23. ¹H NMR (δ, ppm; J, Hz): 7.16 (9H, m), 3.44 (2H, s), 2.50 (2H, m), 2.34 (2H, s), 0.84 (2H, m), 0.03 (6H, s).

Dimethyl(octyl)phenylsilane 24.^{S8} GC-MS (m/z, M⁺ 248.2), major peaks found: 248.2 (<1%), 233.2 (6%), 170.2 (11%), 136.2 (14%), 135.2 (100%), 121.2 (26%), 105.2 (6%). ¹H NMR (δ, ppm; J, Hz): 7.30 (5H, m), 1.17 (14H, m), 0.77 (3H, t, J = 6.7 Hz), 0.58 (6H, s).

2-(Phenylsilyl)bicyclo[2.2.1]heptane 25. ¹H NMR (δ, ppm; J, Hz): 7.88 – 6.67 (m, 5H), 4.20 – 4.00 (m, 2H), 2.51 – 1.60 (m, 2H), 1.60 – 0.37 (m, 9H). ¹³C NMR (δ, ppm; J, Hz): 135.46, 132.79, 129.48, 127.95, 38.84, 37.36, 37.31, 33.77, 33.58, 29.16, 24.22.

Dimethyl(octyloxy)(phenyl)silane 27.^{S9} GC-MS (m/z, M⁺ 264.2), major peaks found: 264.2 (<1%), 251.2 (6%), 250.2 (23%), 249.2 (100%), 186.2 (23%), 137.2 (65%), 135.2 (36%), 121.2 (12%). ¹H NMR (δ, ppm; J, Hz): 7.33 (5H, m), 3.47 (2H, m), 1.38 (4H, m), 1.10 (8H, m), 0.75 (3H, t, J = 5.5 Hz), 0.23 (6H, s).

Benzyl(dimethyl(octyloxy)silane 28.^{S10a} GC-MS (m/z, M⁺ 278.3), major peaks found: 278.3 (6%), 263.2 (2%), 189.2 (5%), 188.2 (18%), 187.3 (100%), 149.2 (19%), 121.2 (11%), 91.2 (10%), 89.2 (11%), 75.2 (51%), 69.2 (17%). ¹H NMR (δ, ppm; J, Hz): 7.12

(2H, t, J = 7.5 Hz), 6.98 (3H, t, J = 7.6 Hz), 3.48 (2H, t, J = 6.7 Hz), 2.10 (2H, s), 1.42 (2H, m), 1.14 (10H, m), 0.81 (3H, t, J = 6.3 Hz), 0.00 (6H, m).

1,1,1,3,3-Pentamethyl-3-(octyloxy)disiloxane 29.^{S10a} GC-MS (m/z, M⁺ 276.1), major peaks found: 276.1 (<1%), 263.1 (5%), 262.1 (12%), 261.1 (45%), 177.1 (6%), 151.1 (8%), 150.1 (16%), 149.1 (100%), 147.1 (28%), 133.1 (31%), 71.2 (11%), 57.2 (12%), 43.2 (8%). ¹H NMR (δ, ppm; J, Hz): 3.55 (2H, t, J = 6.7 Hz), 1.44 (2H, m), 1.12 (10H, m) 0.78 (3H, t, J = 6.6 Hz), 0.00 (15H, s).

Triethyl octyl silicate 31.^{S10a} GC-MS (m/z, M⁺ 292.2), major peaks found: 292.2 (<1%), 247.1 (7%), 150.1 (11%), 149.1 (100%), 137.1 (77%), 135.1 (39%), 119.1 (30%), 105.1 (45%), 91.1 (24%), 69.2 (33%), 63.2 (31%). ¹H NMR (δ, ppm; J, Hz): 3.78 (6H, q, J = 7.0 Hz), 3.69 (2H, t, J = 6.6 Hz), 1.46 (2H, m), 1.15 (19H, m), 0.81 (3H, t, J = 6.7 Hz).

(Hexan-2-yloxy)diphenylsilane 32. GC-MS (m/z, M⁺ 284.2), major peaks found: 284.2 (<1%), 269.1 (3%), 227.2 (50%), 206.2 (23%), 199.2 (21%), 183.2 (100%), 181.2 (25%), 151.2 (10%), 128.1 (15%), 123.2 (47%), 105.2 (25%), 78.3 (9%).

1,1,1,3,3-Pentamethyl-3-(1-phenylethoxy)disiloxane 33. GC-MS (m/z, M⁺ 268.1), major peaks found: 269.1 (9%), 268.1 (35%), 172.2 (10%), 149.1 (44%), 133.1 (12%), 105.2 (100%), 77.2 (7%).

Benzyl dimethyl(phenethoxy)silane 34. GC-MS (m/z, M⁺ 270.1), major peaks found: 270.1 (<1%), 255.2 (2%), 180.2 (17%), 179.2 (100%), 161.2 (20%), 149.2 (7%), 105.3 (27%), 99.2 (13%), 75.2 (21%).

Dimethyl(4-nitrophenoxy)phenylsilane 35. GC-MS (m/z, M⁺ 273.1), major peaks found: 274.1 (7%), 273.1 (33%), 260.1 (6%), 259.1 (22%), 258.1 (100%), 197.2 (11%), 135.2 (30%).

Dimethyl((4-methylpentan-2-yl)oxy)(phenyl)silane 36.^{S10b} ¹H NMR (δ, ppm; J, Hz): 7.66-7.57 (2H, m), 7.44-7.36 (3H, m), 3.96-3.83 (1H, m), 1.76-1.63 (1H, m), 1.51-1.42 (1H, m), 1.25-1.15 (1H, m), 1.14 (d, 3H, J = 6.0 Hz), 0.87 (d, 3H, J = 6.6 Hz), 0.83 (d, 3H, J = 6.6 Hz), 0.36 (s, 6H). ¹³C NMR (δ, ppm; J, Hz): 138.5 (C), 133.5 (2XCH), 129.4 (CH), 127.8 (2CH), 67.2 (CH), 49.0 (CH₂), 24.6 (CH), 24.1 (CH₃), 23.1 (CH₃), 22.4 (CH₃), -1.0 (CH₃), -1.1 (CH₃).

4-acetylphenyl triethyl silicate **37**. ^1H NMR (δ , ppm; J, Hz): 7.89 (2H, d, J = 8.7 Hz), 6.92 (2H, d, J = 8.7 Hz), 3.96-3.72 (6H, m), 2.56 (3H, s), 1.25-1.18 (9H, m). ^{13}C NMR (δ , ppm; J, Hz): 198.0 (C), 161.4 (C), 131.1 (2xCH), 129.6 (C), 115.5 (2xCH), 59.2 (3xCH₂), 26.3 (CH₃), 17.9 (3xCH₃).

4-(Triethylsilyloxy)acetophenone **38**.^{S10b} ^1H NMR (δ , ppm; J, Hz): 7.87 (d, J = 8.5 Hz, 2H), 6.88 (d, J = 8.5 Hz, 2H), 2.55 (s, 3H), 1.00 (t, J = 6.0 Hz, 9H), 0.77 (q, J = 6.0 Hz, 6H); ^{13}C NMR (δ , ppm; J, Hz): 198.5 (C), 161.4 (C), 131.2 (2xCH), 129.6 (C), 115.5 (2xCH), 26.3 (CH₃), 6.8 (3xCH₃), 6.4 (3xCH₂).

Computational details

All designed models were fully optimized at the $\omega\text{B97X-D}$ theory level.^{S11} We have previously shown that this approach provides reliable results for the thermochemistry and kinetics of Pt-based compounds.^{S12} The def2-SVP basis set was used to describe all the atoms, except the Pt centres, where the core electrons were replaced by the effective core potentials to account for scalar relativistic effects^{S13} without increasing the computational cost.^{S12} For all calculations, we used an ultrafine grid for numerical density functional theory integration. The optimized structures were confirmed to be stable (real minima) or transitional state (saddle point) in the potential energy surface by analysing their vibrational modes. No imaginary frequency was obtained for the products and reactants, although a single imaginary frequency was obtained for the transitional state. In addition, relative energy curves along with the reaction were computed by monitoring the hydrosilylation phenomena. This is a relaxed potential energy scan over the oxidative addition. Because solvation might influence the reactivity of Pt compounds,^{S14} environmental effects were included by using the polarizable continuum method of Tomasi and co-workers.^{S15} All calculations were performed with Gaussian16.^{S16}

Graphical method.

General discussion.

The graphical methodology described in the manuscript is applied, in general terms, as follows: 1) Different reactions changing one variable (T, σ_x , etc.) are set and followed kinetically over time. 2) Aliquots are analyzed using an appropriate experimental technique (GC, NMR, IR, etc.) to measure concentration. 3) The corresponding time-scale normalization is applied using a spreadsheet. 4) The desired value is found in an

iterative way giving different values until all kinetic profiles graphically overlay. 5) A more mathematically precise way to obtain the desired value along with the experimental error of the measurement is a) adjusting all the data, [P] vs. t to a polynomial function (depending on the case, normally 3rd grade is enough) and the values of the desired parameter are changed by iteration (for example using Solver function in Excel) until R^2 reach its maximum value, or b) minimizing the accumulated distance between nearest neighbors to ensure best overlay.

Calculation of the error for the graphical method for activation parameters is as follows:

1) Reaction profiles at two temperatures (X and Y) are obtained by GC or other quantitative technique (NMR, etc.). 2) Data points for each temperature are divided into two subsets (X1 and Y1). 3) Activation parameters are calculated for the entire profiles and for the four combinations of the subsets (i.e. X-Y, X1-Y1, X1-Y2, X2-Y1 and X2-Y2). 4) Weighted average of the 5 values is calculated (giving X-Y double the weight of the rest combinations) and error is calculated from the standard deviation. Error is calculated similarly for Hammett and KIE.

The concentration data for the simulated reactions shown in the figures of the manuscript have been calculated by using the theoretical rate equation for each individual kinetic profile (1st order, 2nd order, etc.) and the different kinetic rate constants have been calculated from the corresponding equation addressing the changes in temperature (Eyring-Polanyi), sigma values (Hammett) or kinetic isotopic effect (KIE), as described in the following sections. Numerical data for each simulation is provided at the end of this text.

Simplicity and associated error.

In traditional methodologies, every reaction at a determinate temperature gives one numeric value for rate or kinetic constant. In order to have statistically significant values for activation parameters, reactions have to be carried out at least at three different temperatures. In contrast to that, for this graphical analysis every point of the kinetic profile is a separate value that provides information for the calculation of the required value. For this reason, experiments at only two different temperatures are needed and a lower number of data points are necessary to obtain a more precise results of the desired values, i.e. activation parameters, than for initial rates methodology. In addition, for initial rates methodology, several data points are required to obtain a precise measure of the

initial rate (if possible) that minimize the transfer of uncertainty to the next step for the calculation of the values. However, in our methodology, values are obtained directly from raw concentration data, avoiding the propagation of error from the calculation of initial rates to the calculation of activation parameters.

The biggest limitation of graphical methodologies is that they do not provide a measure of the error associated to the calculated value (order of reagent or catalyst), which makes impossible a direct comparison with other methods in terms of accuracy. We can take advantage of the fact that every point of the kinetic profile is independent from the rest in order to calculate the errors. Data from the two temperatures X and Y are split into two different data sets for each temperature (X1 and X2; Y1 and Y2), as shown in Figure S9, and the activation parameters are calculated using the four possible combinations (X1-Y1, X1-Y2, X2-Y1 and X2-Y2). The correct values are obtained from the weighted average between the four subset combinations and the one calculated using the entire kinetic profiles and the standard deviation gives the measure of the uncertainty associated to the calculation.

In order to adjust the value to make the profiles overlay, three different approaches can be followed: **1) *Visual adjustment*** is the simplest way to adjust the parameters for the overlay of the kinetic profiles and is good for a first approach or to give a rough estimate of the value without associated error, however, it is subjective and carries an unknown uncertainty that can jeopardize the calculation of the error. **2) *Adjustment to a polynomial equation*** of the profile containing both X and Y is an alternative way to obtain the desired values. The procedure consists in changing the desired value (enthalpy, entropy, etc.) until the R^2 given in the adjustment of the equation is maximized. This can be done manually although is more tedious. An optimization algorithm (like Solver® in excel) can give the results much faster and with higher precision. This methodology can be very helpful, however, it is highly dependent on how well the data adjust to the polynomial equation and can produce misleading results. **3) Calculation of *Euclidean distance between consecutive points and minimization*** of the summation of the distances for all the points. This methodology is based in the principle that the best overlay must minimize the distances between consecutive points. The procedure consists in the following steps:

1. Sort the data points by increasing [Product], calculating the function (f, g, etc.) for each point.

2. Normalize the X axis to reach a maximum of 1 (divide every f, g, etc. value for each point between the maximum value).
3. Calculate the Euclidean distance between each consecutive pair of data points (defined as $[(x_i - x_{i+1})^2 + (y_i - y_{i+1})^2]^{1/2}$).
4. Calculate the summation of all the distances and change the value of the parameter (enthalpy, entropy, etc.) until finding the minimum value.

This latter method is the least biased of all three and therefore have been used throughout this work. Figure S19c shows the application of the methodology for the calculation of Hammett parameters.

Enthalpy value.

Eyring-Polanyi equation (Eq. 1) was used to extract the dependence of the kinetic constant with respect to temperature through activation parameters (transition state enthalpy and entropy).

$$[\text{Eq. (1)}] \quad k(T) = \frac{k_B T}{h} e^{\Delta S^\ddagger/R} e^{-\Delta H^\ddagger/RT}$$

Reaction rate depends on concentration of the reagents and on the kinetic constant and therefore on reaction temperature. We can describe a function f to include the rate dependence with respect to all the parameters but kinetic constant and then integrate the inverse of this function to obtain the time dependence. Then, constant values are removed from the equation to get the normalized time-scale f that depends on time, temperature and transition state entropy. Time and temperature are known for each point of the kinetic profiles, remaining ΔH^\ddagger as the only unknown variable that is calculated iteratively from the overlay of the kinetic profiles:

$$-\frac{d[A]}{dt} = f([A], [B], \dots)k(T, \Delta H^\ddagger, \Delta S^\ddagger); \quad k(T, \Delta H^\ddagger, \Delta S^\ddagger) = \frac{k_B T}{h} e^{\Delta S^\ddagger/R} e^{-\Delta H^\ddagger/RT}$$

$$\int_{[A]_0}^{[A]_t} f^{-1}([A], [B], \dots)d[A] = \int_0^t -kdt$$

$$F^{-1}([A]_t, [A]_0, [B]_0, \dots) = -kt = -t \frac{k_B T}{h} e^{\Delta S^\ddagger/R} e^{-\Delta H^\ddagger/RT}$$

$$[\text{Eq. (2)}] \quad f(t, T, \Delta H^\ddagger) = tT e^{-\Delta H^\ddagger/RT}$$

Entropy value.

Entropy appears in an exponential term that is not altered by temperature changes in Eq. (1), so cannot be calculated from the aforementioned time-scale normalization. For entropy calculation, we must perform a mathematical transformation to include dependence of T in the entropy term by raising k to the power of T/T_m (T_m = average T used in measurements). Thus, if we simply raise Eq. (1) to the power of temperature, divided by average temperature of the experiments to have a manageable data, we obtain Eq. (3) where temperature dependence affects the entropy term.

$$[\text{Eq. (3)}] \quad k^{T/T_m}(T) = \left(\frac{k_B T}{h}\right)^{T/T_m} e^{T\Delta S^\ddagger/RT_m} e^{-\Delta H^\ddagger/RT_m}$$

After performing an approximation (T/T_m ≈ 1), g can be defined as follows:

$$\begin{aligned} \left(-\frac{d[A]}{dt}\right)^{T/T_m} &= f^{T/T_m}([A], [B], \dots) k^{T/T_m}(T, \Delta H^\ddagger, \Delta S^\ddagger); k^{T/T_m} \\ &= \left(\frac{k_B T}{h}\right)^{T/T_m} e^{T\Delta S^\ddagger/RT_m} e^{-T\Delta H^\ddagger/R} \end{aligned}$$

$$\left(-\frac{d[A]}{dt}\right)^{T/T_m} = -\frac{d^{T/T_m}[A]}{dt^{T/T_m}} \approx -\frac{d[A]}{dt}$$

$$\int_{[A]_0}^{[A]_t} f^{-T/T_m}([A], [B], \dots) d[A] = \int_0^t -k^{T/T_m} dt$$

$$G^{-1}([A]_t, [A]_0, [B]_0, \dots) = -k^{T/T_m} t = -t \left(\frac{k_B T}{h}\right)^{T/T_m} e^{T\Delta S^\ddagger/RT_m} e^{-T\Delta H^\ddagger/R}$$

$$[\text{Eq. (4)}] \quad g(t, T, \Delta H^\ddagger) = t \left(\frac{k_B T}{h}\right)^{T/T_m} e^{T\Delta S^\ddagger/RT_m}$$

A new normalized time-scale g(t, T, ΔS[‡]) Eq. (4) is obtained and ΔS[‡] is calculated directly by overlying product concentration profiles at different temperatures representing concentration versus g at the correct ΔS[‡] value, as shown in Figure 3 in the main text.

ΔH^\ddagger and ΔS^\ddagger can be calculated analogously for any reaction by applying the simple graphical method using the corresponding normalized time-scales in Eq. 2 and 4.

Now we can compare the graphical method with the initial rates in terms of error of the measurements to check if it is really superior. For that, 2% random error was included in the concentration data from the reaction in Figure 2 and both methods were applied (Figure S9). For the initial rates method, we used the data from the three different temperatures, obtaining values of $57 \pm 3 \text{ KJ}\cdot\text{mol}^{-1}$ and $-152 \pm 8 \text{ J}\cdot\text{K}^{-1}\cdot\text{mol}^{-1}$ for the enthalpy and entropy, respectively. Which involve a deviation from the real values of 14 and 11%, respectively. On the other hand, the graphical method only needs two temperatures (highest and lowest), obtaining a value of $51.8 \pm 1.3 \text{ KJ}\cdot\text{mol}^{-1}$ and $-169 \pm 4 \text{ J}\cdot\text{K}^{-1}\cdot\text{mol}^{-1}$ for the enthalpy and entropy, respectively. These values have much lower uncertainty and are much closer to the real values (50 and -170) than the calculated by initial rates method, confirming that our methodology is more precise using less data and experiments. The complete mathematical development is as follows:

A second order reaction is simulated in which two different compounds (A and B) react with each other in just one-step to give the product (P) at different temperatures according to Eq. (S1).



Concentration of the reagents and product is calculated from the kinetic rate equation: Eq. (S2) and (S3) with initial concentrations of $[\text{A}]_0 = [\text{B}]_0 = 1.0 \text{ M}$. Kinetic constants at different temperatures are calculated using Eyring-Polanyi equation: Eq. (S4) with transition state activation parameters $\Delta H^\ddagger = 50 \text{ KJ}\cdot\text{mol}^{-1}$ and $\Delta S^\ddagger = -170 \text{ J}\cdot\text{K}^{-1}\cdot\text{mol}^{-1}$, as shown in Tables S1-S5.

$$\text{[Eq. (S2)]} \quad \frac{d[\text{P}]}{dt} = k_2(T)[\text{A}][\text{B}]$$

$$\text{[Eq. (S3)]} \quad \frac{1}{[\text{A}]} = \frac{1}{[\text{A}]_0} + k_2(T)t$$

$$\text{[Eq. (S4)]} \quad k_2(T) = \frac{k_B T}{h} e^{\Delta S^\ddagger/R} e^{-\Delta H^\ddagger/RT}$$

Hammett parameter.

Another powerful tool to extract information about organic reaction mechanisms are Linear Free Energy Relationships (*LFER*),³ based on electronic effects on a reactive functionality from different substituents. Hammett plot (Eq. 5) is a representative example of LFER and indicates how reaction rate and kinetic constant are affected by the electronic nature of a substituent (-X) linked to a reactive functionality, giving electronic information about the rate-determining step (rds) of the reaction. Application of the graphical methodology for Eq. 5 simply consists on representing product concentrations versus the normalized time-scale $h(t, \rho, \sigma_X)$ Eq. (6), for reactions with different substituents (change in σ_X), and ρ is calculated iteratively until all profiles overlay. Please note that this analysis can be applicable to other LFERs, like Taft equation.

$$[\text{Eq. (5)}] \quad \log\left(\frac{k_X}{k_H}\right) = \rho\sigma_X$$

$$[\text{Eq. (6)}] \quad h(t, \sigma_X, \rho) = te^{\rho\sigma_X}$$

Figure S19 and Table S10 shows the application of the described methodology compared to initial rates method in a simulated bimolecular reaction $A+B \rightarrow P$ of aromatic compounds with different substituents with a $\rho = 0.50$. The advantage of the graphical methodology is more evident for this fast reaction ($t_{1/2} = 40 - 90$ s), where a reliable measure of initial rate (lower than 20% conversion) is technically difficult to obtain. Indeed, while the classical initial rates method gives a ρ value of 0.40 (Figure S19a), which supposes a 20% deviation from the correct value (0.50), the graphical method gives the exact value $\rho = 0.50$ (Figure S19b). The mathematical development is as follows:

A bimolecular reaction of different *para*-substituted aromatic compounds A_X with B is shown to obtain product P_X (Eq. S5) and the methodology described in the paper is compared with the traditional initial rates methodology to obtain Hammett parameter rho (ρ).



Concentration of the reagents and product is calculated from the kinetic rate equation: Eq. (6) and (7) with initial concentrations of $[A_X]_0 = 0.6$ and $[B]_0 = 0.5$ M. Kinetic constants at different temperatures are calculated using Hammett equation: Eq. (8) with rho parameter equal to 0.5.

$$\text{[Eq. (S6)]} \quad \frac{d[P]}{dt} = k_X[A_X][B]$$

$$\text{[Eq. (S7)]} \quad \ln \frac{[A]}{[B]} = \ln \frac{[A]_0}{[B]_0} + k_X([A]_0 - [B]_0)t$$

$$\text{[Eq. (S8)]} \quad \log \left(\frac{k_X}{k_H} \right) = \rho \sigma_X$$

The initial rate method was carried out for comparison with the graphical analysis reported in the main text. For this, linear regression of the first three data points was performed in each case and the results for the slopes measured are presented in Table S7, the value of ρ is calculated using linear regression from the second (x) and fifth (y) columns of Table S10. Numeric data for the kinetic graphical analysis method is shown in Table S10.

KIE values.

Kinetic isotopic effects (*KIE*) are measured in organic chemistry to extract information about bond breaking/formation (or rehybridization) during the rds. These experiments normally involve comparison of the reaction rate for one of the reagents with the deuterated analogue k_H/k_D Eq. (7). Again, measurements must be performed at low conversions with intrinsic experimental errors, and analogously to the previous examples in the work, we can use the graphical method to calculate *KIE* by representing $[P]$ vs. $t \cdot KIE^{-1}$ Eq. (8) for both reactions (with $-H$ and with $-D$) and iterating *KIE* different values until kinetic profiles overlay (see also Table S11).

$$\text{[Eq. (7)]} \quad \left(\frac{k_H}{k_D} \right) = KIE$$

$$\text{[Eq. (8)]} \quad i(t, KIE) = t(KIE)^{-1}$$

Hydrosilylation of alkynes. Kinetic experiments.

Table S1. Kinetic constants $k_2(T)$ calculated at different temperatures for Figure 3 in the main text.

T (°C)	60	80	100
$k_2(T)$ ($M^{-1}\cdot s^{-1}$)	0.000138	0.000406	0.00107

Table S2. Initial rates of reaction shown in Figure S9 calculated by linear regression.

T (°C)	r_0 (P)	r^2
60	$0.776\cdot 10^{-4}$	0.9997
70	$1.301\cdot 10^{-4}$	0.992
80	$2.448\cdot 10^{-4}$	0.995

Table S3. Numeric data for Figure 3a in the main text (transition state enthalpy).

T (°C)	time (s)	[P] (M)	f(t, T, 0)	f(t, T, 10)	f(t, T, 100)	f(t, T, 50)
60 °C	1000	0.1213	333000	9033	7.19E-11	0.00489
	2000	0.2163	666000	18067	1.44E-10	0.00978
	3000	0.2928	999000	27100	2.16E-10	0.01468
	4000	0.3557	1332000	36134	2.87E-10	0.01957
	5000	0.4083	1665000	45167	3.59E-10	0.02446
	6000	0.4529	1998000	54201	4.31E-10	0.02935
	8000	0.5247	2664000	72267	5.75E-10	0.03914
	10000	0.5798	3330000	90334	7.19E-10	0.04892
	12000	0.6235	3996000	108401	8.62E-10	0.05870
	15000	0.6743	4995000	135501	1.08E-09	0.07338
18000	0.7130	5994000	162602	1.29E-09	0.08806	
80 °C	200	0.0752	70600	2349	1.18E-10	0.00288
	400	0.1398	141200	4699	2.35E-10	0.00576
	600	0.1960	211800	7048	3.53E-10	0.00864
	800	0.2454	282400	9398	4.70E-10	0.01153
	1200	0.3278	423600	14097	7.06E-10	0.01729
	1600	0.3940	564800	18796	9.41E-10	0.02305
	2000	0.4484	706000	23495	1.18E-09	0.02882
	3000	0.5494	1059000	35242	1.76E-09	0.04322

T (°C)	time (s)	[P] (M)	f(t, T, 0)	f(t, T, 10)	f(t, T, 100)	f(t, T, 50)
4000		0.6191	1412000	46990	2.35E-09	0.05763
5000		0.6702	1765000	58737	2.94E-09	0.07204
6000		0.7092	2118000	70484	3.53E-09	0.08645
100 °C	80	0.0788	29840	1192	3.08E-10	0.00303
	160	0.1461	59680	2384	6.16E-10	0.00607
	240	0.2042	89520	3575	9.25E-10	0.00910
	320	0.2549	119360	4767	1.23E-09	0.01213
	520	0.3573	193960	7747	2.00E-09	0.01971
	720	0.4350	268560	10726	2.77E-09	0.02729
	920	0.4959	343160	13706	3.54E-09	0.03488
	1120	0.5450	417760	16685	4.32E-09	0.04246
	1520	0.6191	566960	22644	5.86E-09	0.05762
	1920	0.6725	716160	28603	7.40E-09	0.07279
	2320	0.7127	865360	34562	8.94E-09	0.08795

Table S4. Numeric data for Figure 3b in the main text (transition state entropy).

T (°C)	time (s)	[P] (M)	g(t, T, 0)	g(t, T, 100)	g(t, T, -100)	g(t, T, -170)
60 °C	1000	0.1213	6.94E+15	1.14E+21	4.21E+10	9393019
	2000	0.2163	1.39E+16	2.29E+21	8.42E+10	18786039
	3000	0.2928	2.08E+16	3.43E+21	1.26E+11	28179058
	4000	0.3557	2.78E+16	4.57E+21	1.68E+11	37572077
	5000	0.4083	3.47E+16	5.71E+21	2.11E+11	46965097
	6000	0.4529	4.16E+16	6.86E+21	2.53E+11	56358116
	8000	0.5247	5.55E+16	9.14E+21	3.37E+11	75144155
	10000	0.5798	6.94E+16	1.14E+22	4.21E+11	93930193
	12000	0.6235	8.33E+16	1.37E+22	5.05E+11	112716232
	15000	0.6743	1.04E+17	1.71E+22	6.32E+11	140895290
	18000	0.7130	1.25E+17	2.06E+22	7.58E+11	169074348
80 °C	200	0.0752	1.20E+16	4.06E+21	3.54E+10	4758762
	400	0.1398	2.50E+16	8.47E+21	7.37E+10	9922105
	600	0.1960	3.84E+16	1.30E+22	1.13E+11	15250046
	800	0.2454	5.21E+16	1.77E+22	1.54E+11	20687771
	1200	0.3278	8.01E+16	2.71E+22	2.36E+11	31796624
	1600	0.3940	1.09E+17	3.68E+22	3.21E+11	43134382
	2000	0.4484	1.38E+17	4.66E+22	4.06E+11	54645451
	3000	0.5494	2.12E+17	7.17E+22	6.24E+11	83988790
	4000	0.6191	2.87E+17	9.72E+22	8.47E+11	113936766
	5000	0.6702	3.64E+17	1.23E+23	1.07E+12	144342533
	6000	0.7092	4.41E+17	1.49E+23	1.30E+12	175118166
100 °C	80	0.0788	3.72E+16	2.59E+22	5.34E+10	4334018
	160	0.1461	8.09E+16	5.64E+22	1.16E+11	9420641

240	0.2042	1.27E+17	8.88E+22	1.83E+11	14836239
320	0.2549	1.76E+17	1.23E+23	2.52E+11	20477183
520	0.3573	3.03E+17	2.11E+23	4.34E+11	35273724
720	0.4350	4.36E+17	3.04E+23	6.25E+11	50787513
920	0.4959	5.74E+17	4.00E+23	8.23E+11	66834346
1120	0.5450	7.15E+17	4.99E+23	1.03E+12	83308973
1520	0.6191	1.01E+18	7.02E+23	1.44E+12	117286586
1920	0.6725	1.31E+18	9.12E+23	1.88E+12	152367763
2320	0.7127	1.62E+18	1.13E+24	2.32E+12	188344148

Table S5. Numeric data for Figure S9.

T (°C)	time (s)	[P] (M)	g(t, T, 0)	g(t, T, 100)
60 °C	1000	0.1183	0.0023	11615534
	2000	0.1998	0.0045	23231067
	3000	0.2834	0.0068	34846601
	4000	0.3366	0.0090	46462134
	5000	0.4036	0.0113	58077668
	6000	0.4645	0.0135	69693201
	8000	0.5162	0.0180	92924268
	10000	0.5867	0.0225	116155335
	12000	0.6165	0.0270	139386402
	15000	0.6689	0.0338	174233003
18000	0.6995	0.0405	209079604	
80 °C	200	0.0653	0.0014	5960291
	400	0.1269	0.0028	12427316
	600	0.2111	0.0042	19100497
	800	0.2494	0.0055	25911182
	1200	0.3261	0.0083	39824886
	1600	0.4097	0.0111	54025289
	2000	0.4291	0.0139	68442763
	3000	0.5331	0.0208	105194939
	4000	0.6269	0.0277	142704416
	5000	0.6819	0.0346	180787270
6000	0.7137	0.0416	219333375	
100 °C	80	0.0760	0.0015	5497988
	160	0.1625	0.0030	11950706
	240	0.2224	0.0045	18820750
	320	0.2481	0.0061	25976660
	520	0.3695	0.0099	44747051
	720	0.4423	0.0136	64427316
	920	0.4891	0.0174	84783785

1120	0.5482	0.0212	105682939
1520	0.6326	0.0288	148785786
1920	0.6739	0.0364	193288577
2320	0.7180	0.0440	238926999

Table S6. Numeric data for Figure S10 (transition state enthalpy and entropy).

T (°C)	time (s)	[C] (M)	[P] (M)	f(t, T, 54)	g(t, T, -150)
60 °C	333	100	0.0005	2408162	7442264
	333	200	0.0018	4816324	14673624
	333	300	0.0040	7224485	21827462
	333	400	0.0069	9632647	28931417
	333	500	0.0106	12040809	35998509
	333	600	0.0149	14448971	43036362
	333	700	0.0198	16857133	50049994
	333	800	0.0252	19265294	57042956
	333	900	0.0311	21673456	64017898
	333	1000	0.0373	24081618	70976868
	333	1500	0.0729	36122427	105580249
	333	2000	0.1116	48163236	139942346
	333	2500	0.1496	60204045	174126134
	333	3500	0.2173	84285663	242093693
	333	4500	0.2711	108367281	309656965
	333	5500	0.3128	132448899	376909219
	333	7500	0.3703	180612135	510695614
	333	9500	0.4063	228775372	643740500
	333	11500	0.4301	276938608	776205606
	333	13500	0.4466	325101844	908194824
70 °C	343	30	0.0001	1313083	3660441
	343	60	0.0006	2626166	7365795
	343	90	0.0013	3939250	11088291
	343	120	0.0023	5252333	14821964
	343	150	0.0035	6565416	18563970
	343	180	0.0050	7878499	22312629
	343	240	0.0087	10504666	29825786
	343	300	0.0132	13130832	37355710
	343	360	0.0184	15756998	44899024
	343	560	0.0402	24510886	70115741
	343	760	0.0663	33264774	95413828
	343	960	0.0943	42018662	120771421
	343	1160	0.1225	50772550	146176012
	343	1660	0.1880	72657270	209845467
	343	2160	0.2423	94541990	273687011

	343	2660	0.2856	116426709	337660272
	343	3160	0.3198	138311429	401740356
	343	4160	0.3689	182080869	530157967
	343	5160	0.4012	225850309	658850926
	343	6160	0.4236	269619748	787765531
T (°C)	time (s)	[C] (M)	[P] (M)	f(t, T, 54)	g(t, T, -150)
80 °C	353	10	0.0001	769686	1872767
	353	20	0.0002	1539371	3846128
	353	30	0.0005	2309057	5859329
	353	40	0.0009	3078742	7898847
	353	50	0.0013	3848428	9958160
	353	70	0.0026	5387799	14121941
	353	90	0.0042	6927170	18332092
	353	110	0.0061	8466541	22578465
	353	160	0.0123	12314969	33315294
	353	210	0.0203	16163396	44183338
	353	260	0.0296	20011824	55151719
	353	360	0.0511	27708680	77320022
	353	460	0.0750	35405535	99728124
	353	560	0.0998	43102390	122324737
	353	760	0.1483	58496101	167961922
	353	960	0.1922	73889812	214066022
	353	1160	0.2302	89283523	260541512
	353	1660	0.3024	127767800	377988298
	353	2160	0.3505	166252077	496816554
	353	2660	0.3836	204736354	616710696

Table S7. Numeric data for Figure S11 (transition state enthalpy and entropy).

T (°C)	time (s)	[P] (M)	f(t, T, 55.5)	g(t, T, -148)
60 °C	300	0.0024	4205505	27617870
	600	0.0096	8411010	54453085
	900	0.0222	12616515	81000620
	1500	0.0671	21027525	133588668
	2500	0.1462	35045875	220318464
	3500	0.2084	49064225	306316515
	5500	0.3066	77100925	476896019
	7500	0.3754	105137626	646173383
	9500	0.3970	133174326	814512531
	13500	0.4368	189247726	1149121524
T (°C)	time (s)			
70 °C	90	0.0088	2329570	14129286
	180	0.0107	4659139	28431932
	360	0.0248	9318279	57212709

	760	0.0759	19671922	121581343
	1160	0.1172	30025566	186265200
	1660	0.1967	42967620	267396184
	2660	0.2822	68851728	430264564
	3160	0.3169	81793782	511918794
	4160	0.3759	107677891	675555301
	6160	0.4239	159446107	1003812474
T (°C)	time (s)			
80 °C	30	0.0077	1385989	7519210
	70	0.0076	3233973	18122524
	160	0.0219	7391939	42753132
	260	0.0335	12011900	70775565
	460	0.0715	21251824	127979951
	560	0.1056	25871786	156977924
	960	0.2021	44351633	274708457
	1160	0.2211	53591556	334349917
	1660	0.2924	76691365	485068023
	2660	0.3870	122890982	791417722

Table S8. Kinetic constants $k_2(T)$ calculated at different temperatures for Figure S19.

X	-NH ₂	-OMe	-H	-Br	-CN
σ_x	-0.660	-0.268	0.000	0.232	0.660
K_x (M ⁻¹ ·s ⁻¹)	0.0180	0.0219	0.0250	0.0281	0.0348

Table S9. Initial rates of reaction shown in Figure S19 calculated by linear regression.

X	σ_x	r_0 (P _x)	r^2	$\ln(r_0(P_x)/r_0(P_H))$
-NH ₂	-0.660	0.00458	0.998	-0.273
-OMe	-0.268	0.00540	0.998	-0.109
-H	0.000	0.00602	0.997	0.000
-Br	0.232	0.00661	0.997	0.092
-CN	0.660	0.00779	0.996	0.257

Table S10. Numeric data for Figure S19 (Hammett).

-X	time (s)	[P] (M)	h(t, σ_x, 0)	h(t, σ_x, -1)	h(t, σ_x, 0.5)
-NH₂	10	0.0491	10	19.35	7.19
	20	0.0900	20	38.70	14.38
	30	0.1247	30	58.04	21.57
	40	0.1545	40	77.39	28.76
	50	0.1803	50	96.74	35.95
	70	0.2229	70	135.44	50.32
	90	0.2565	90	174.13	64.70
	110	0.2837	110	212.83	79.08
	160	0.3333	160	309.57	115.03
	210	0.3667	210	406.31	150.97
	260	0.3907	260	503.05	186.92
	360	0.4226	360	696.53	258.81
	-OMe	10	0.0586	10	13.07
20		0.1057	20	26.15	17.49
30		0.1446	30	39.22	26.24
40		0.1771	40	52.29	34.98
50		0.2047	50	65.37	43.73
70		0.2490	70	91.51	61.22
90		0.2831	90	117.66	78.71
110		0.3100	110	143.81	96.20
160		0.3577	160	209.18	139.93
210		0.3888	210	274.54	183.66
260		0.4106	260	339.91	227.39
360		0.4389	360	470.64	314.85
-H		10	0.0659	10	10
	20	0.1176	20	20	20
	30	0.1592	30	30	30
	40	0.1934	40	40	40
	50	0.2221	50	50	50
	70	0.2672	70	70	70
	90	0.3011	90	90	90
	110	0.3275	110	110	110
	160	0.3734	160	160	160
	210	0.4028	210	210	210
	260	0.4230	260	260	260
	360	0.4488	360	360	360
	-Br	10	0.0730	10	7.93
20		0.1287	20	15.86	22.46
30		0.1726	30	23.79	33.69
40		0.2081	40	31.72	44.92

	50	0.2374	50	39.65	56.15
	70	0.2829	70	55.51	78.61
	90	0.3165	90	71.37	101.07
	110	0.3423	110	87.22	123.53
	160	0.3864	160	126.87	179.68
	210	0.4141	210	166.52	235.83
	260	0.4329	260	206.17	291.98
	360	0.4565	360	285.46	404.28
-X	time (s)	[P] (M)	h(t, σ_x, 0)	h(t, σ_x, -1)	h(t, σ_x, 0.5)
-CN	10	0.0876	10	5.17	13.91
	20	0.1509	20	10.34	27.82
	30	0.1987	30	15.51	41.73
	40	0.2362	40	20.67	55.64
	50	0.2663	50	25.84	69.55
	70	0.3116	70	36.18	97.37
	90	0.3440	90	46.52	125.19
	110	0.3683	110	56.85	153.01
	160	0.4085	160	82.70	222.55
	210	0.4329	210	108.54	292.10
	260	0.4491	260	134.38	361.65
	360	0.4687	360	186.07	500.75

Table S11. Numeric data for Figure 4 in the main text (*KIE*).

	time (s)	i(t, 1.91)	[P] (M)
HSiEt₃	0.5	0.5	0.019
	1	1	0.031
	2	2	0.055
	5	5	0.097
	10	10	0.152
	20	20	0.231
	40	40	0.403
	DSiEt₃	0.5	0.26
1		0.52	0.021
2		1.05	0.033
5		2.62	0.060
10		5.24	0.099
20		10.47	0.153
40		20.94	0.243

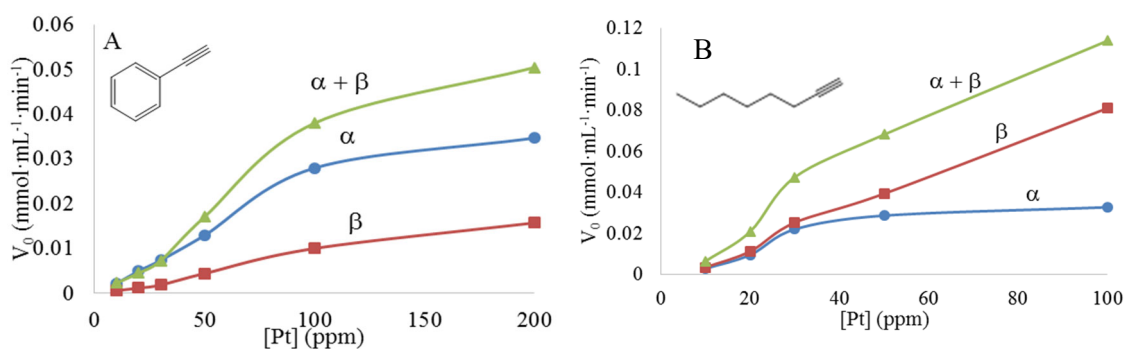


Figure S1. Effect of catalyst concentration on hydrosilylation reaction rate. [Pt] is given in ppm with respect to the alkyne. Reaction conditions: alkyne 0.5 mmol, HSiEt₃ 0.6 mmol, toluene 1 mL, 110 °C.

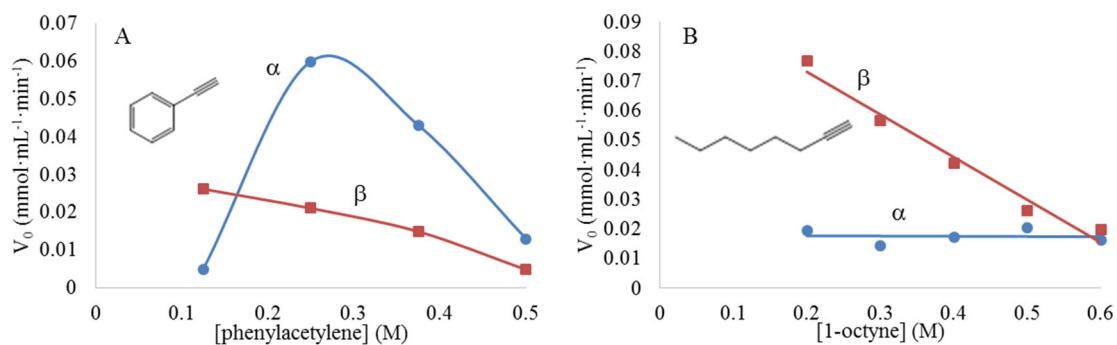


Figure S2. Reaction rate for different alkyne concentrations: A) phenylacetylene, B) 1-Octyne, HSiEt₃ 0.6 mmol, 1 mL of toluene and $2.5 \cdot 10^{-5}$ mmol Pt.

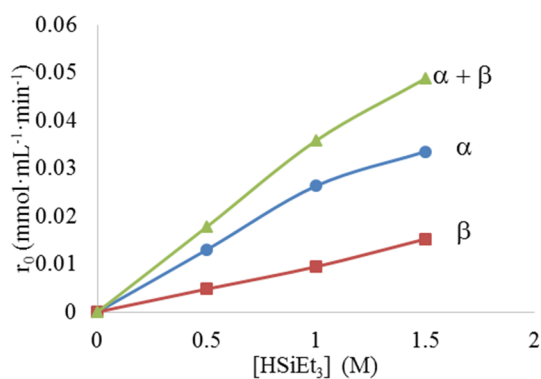


Figure S3. Reaction rate for different silane concentrations. Phenylacetylene 0.5 mmol, 0.6 mmol of HSiEt₃, 1 mL of toluene and $2.5 \cdot 10^{-5}$ mmol Pt Karstedt, 110 °C.

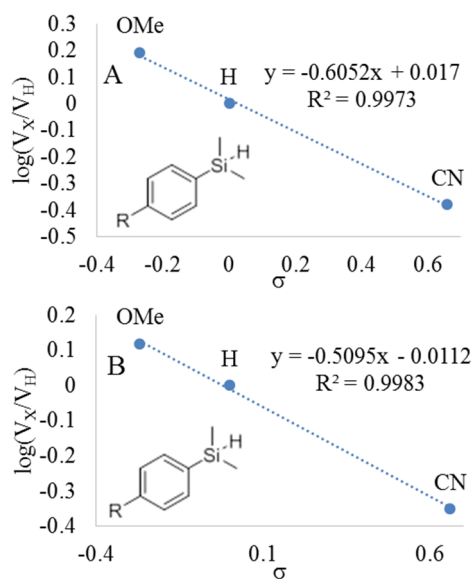


Figure S4. Hammett plots for para-substituted dimethylphenylsilanes. A) α -alkenylsilane B) β -alkenylsilane. Reaction conditions: phenylacetylene 0.5 mmol, *p*-R-PhMe₂SiH 0.6 mmol (R= OMe, H, CN), Pt Kardstedt 0.005 mol%, 1 mL of toluene, 110 °C.

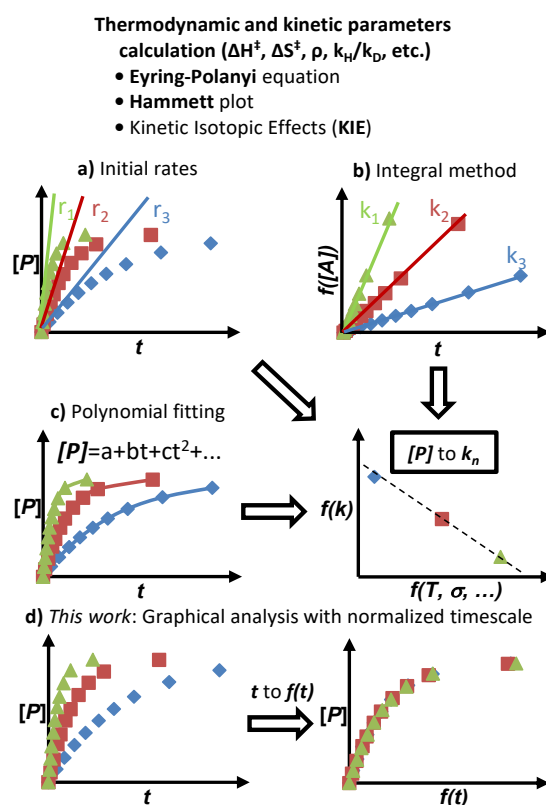
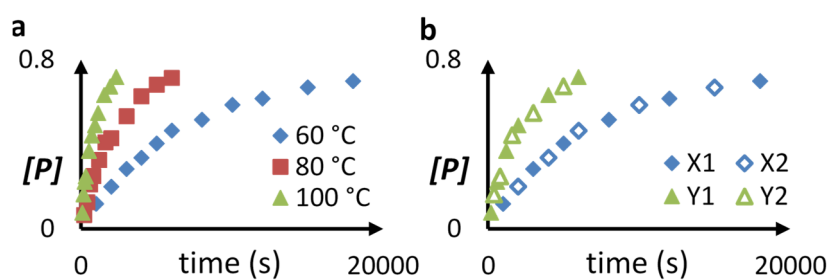


Figure S5. Comparison of **a-c)** traditional methods to measure reaction kinetics based on concentration measurements and subsequent transformation to rate with **d)** the graphical analysis described in this work that uses concentration profiles to calculate different thermodynamic and kinetic parameters of chemical reactions.



c

Graphical analysis method		
Data set	ΔH^\ddagger (KJmol ⁻¹)	ΔS^\ddagger (JK ⁻¹ mol ⁻¹)
X-Y	51.26	-171.4
X1-Y1	50.52	-172.9
X1-Y2	53.85	-163.2
X2-Y1	51.18	-170.4
X2-Y2	53.06	-166.4
Average	51.8 ± 1.3	-169 ± 4
Initial rates method		
ΔH^\ddagger (KJmol ⁻¹)	ΔS^\ddagger (JK ⁻¹ mol ⁻¹)	R ²
57 ± 3	-152 ± 8	0.997

Figure S6. a) Kinetic profiles, b) application of the graphical method with split of data in four subsets and c) comparison of initial rates method with the graphical method for a simulated bimolecular reaction. $R^2 > 0.999$ for the graphical method.

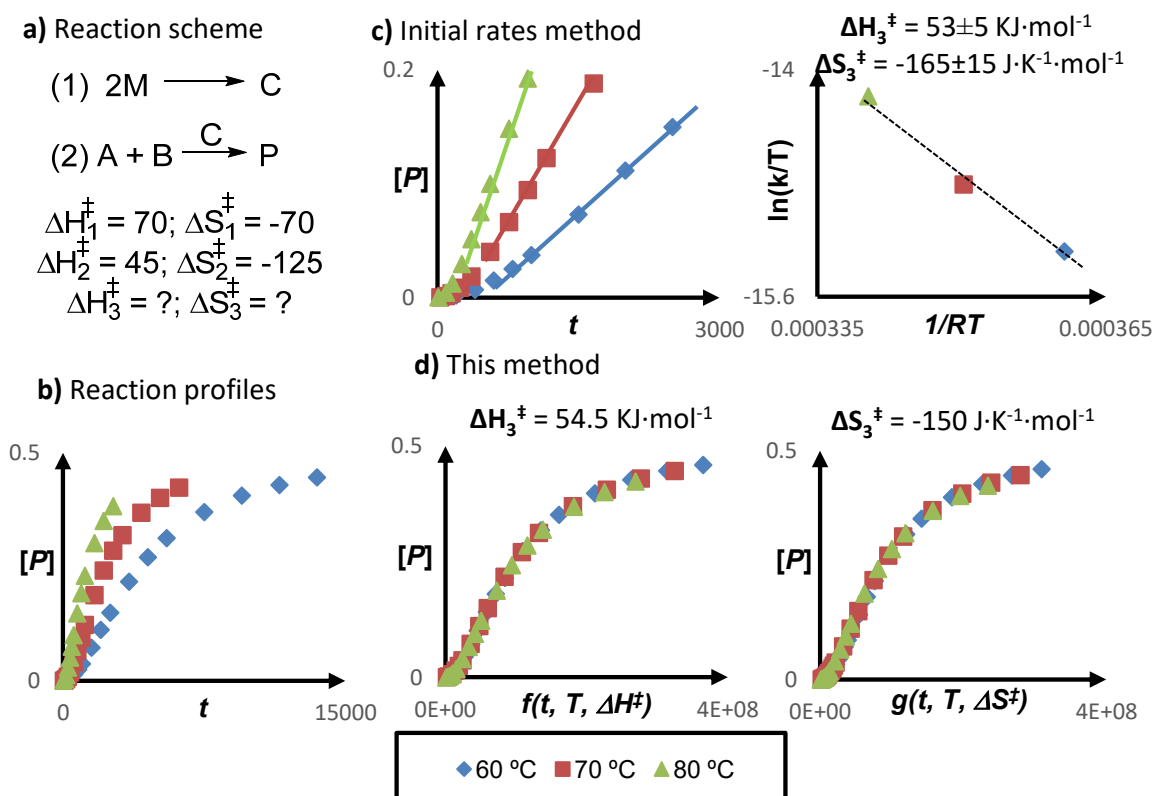
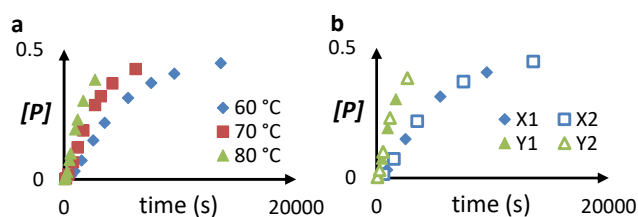
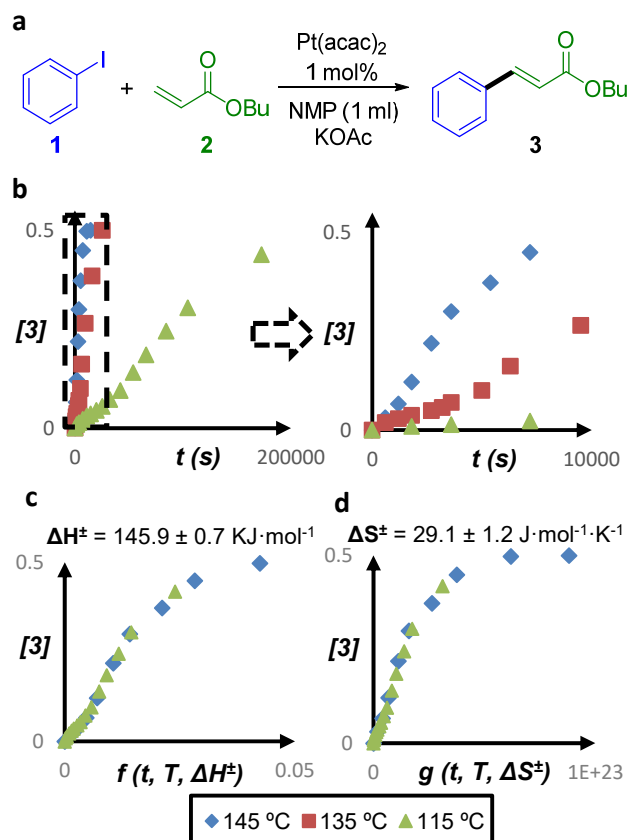


Figure S7. Simulation of a reaction with an induction time: a) chemical reaction involving two processes: (1) *in-situ* formation of active species by metal aggregation and (2) catalytic cycle in which reagents A and B form P catalysed by the active species; (3) correspond to the whole process (1) + (2). b) Reaction profile. c) Transition state enthalpy and entropy calculation by initial rates, in this case measuring the rate after the induction time. d) Transition state enthalpy and entropy calculation by the graphical method.



Method	ΔH^\ddagger (KJmol ⁻¹)	ΔS^\ddagger (JK ⁻¹ mol ⁻¹)
Initial rates	53 ± 4	-165 ± 12
Graphical	55.5 ± 1.0	-148 ± 4

Figure S8. Comparison of the graphical method (a) with the initial rates method (b) by introducing 2% random error in a simulated example of a reaction with induction time (from Figure S10) caused by in-situ catalyst formation. For the initial rates method, rate is measured after induction time at three different temperatures to obtain the activation parameters. For the graphical method, only two temperatures are necessary (the lowest and the highest) and data from concentration profile is divided into two subsets for each temperature. Activation parameters are calculated for the whole profiles and for each subset combination and the value is calculated from the weighted average with the error obtained from the standard deviation.



Graphical analysis method			
N	ΔH^\ddagger (KJmol ⁻¹)	ΔS^\ddagger (JK ⁻¹ mol ⁻¹)	
20	145.9 ± 0.7	29.1 ± 1.2	
10	146 ± 2	32.1 ± 1.3	
Initial rates method			
N	ΔH^\ddagger (KJmol ⁻¹)	ΔS^\ddagger (JK ⁻¹ mol ⁻¹)	R ²
60	147 ± 2	28 ± 5	0.999
60 ^a	134 ± 14	-10 ± 35	0.989
30	139 ± 3	6 ± 7	0.992
20	130 ± 16	-19 ± 38	0.986

Figure S9. Graphical analysis method to calculate activation parameters in the Heck reaction catalysed by Pt(acac)₂ that form the clusters *in-situ* under reaction conditions: a) Reaction scheme, b) Reaction profiles, and calculation of c) enthalpy and d) entropy. The Table at the bottom shows the results with different number of data points (N). ^a Measured initial rate instead of rate after induction time.

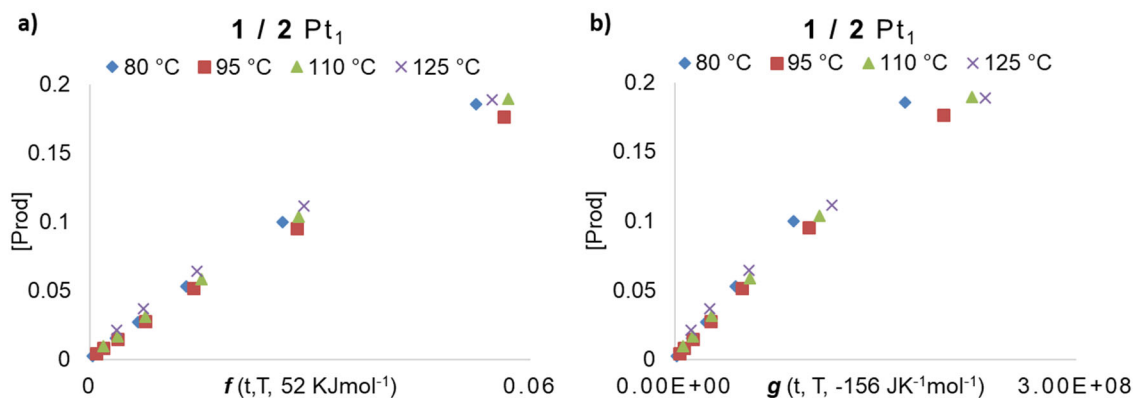


Figure S10. Application of the graphical method to the calculation of transition state enthalpy (a) and entropy (b) of phenylacetylene **1** and triethylsilane **2** catalysed by Pt₁ (Table 1, entry 1 in the main text).

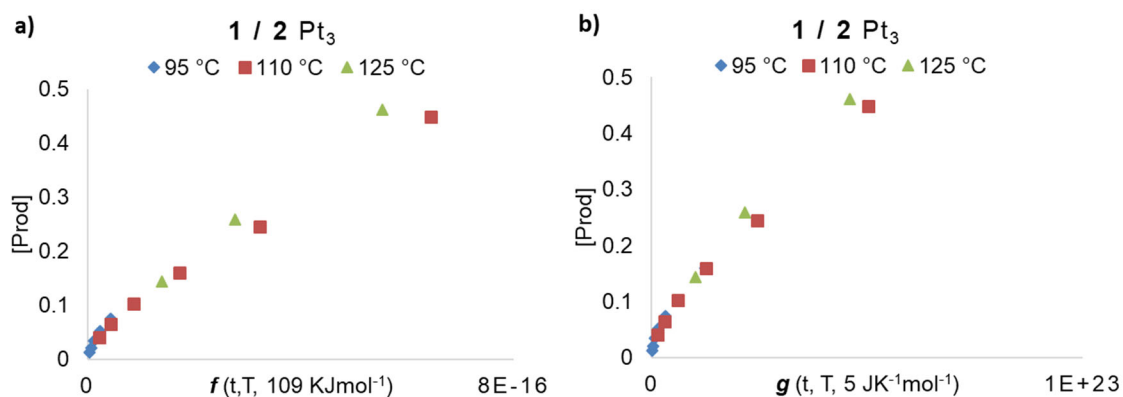


Figure S11. Application of the graphical method to the calculation of transition state enthalpy (a) and entropy (b) of phenylacetylene **1** and triethylsilane **2** catalysed by Pt₃ (Table 1, entry 2 in the main text).

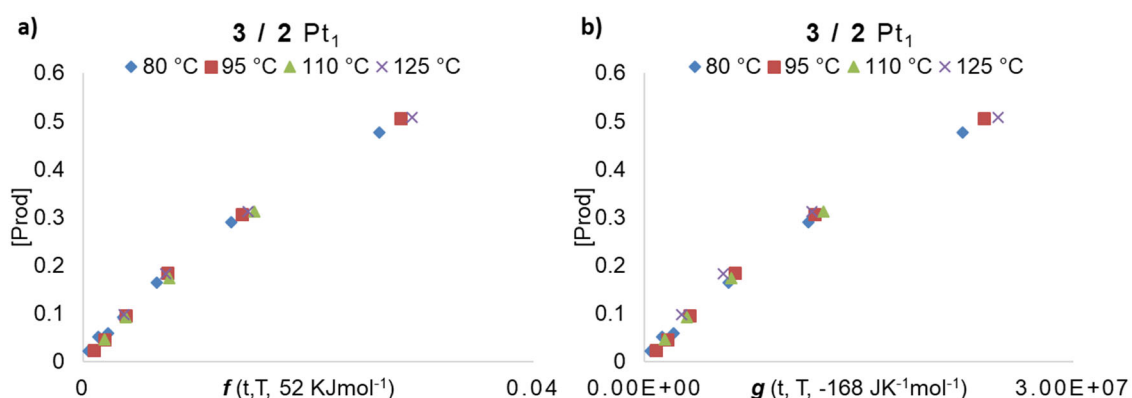


Figure S12. Application of the graphical method to the calculation of transition state enthalpy (a) and entropy (b) of 1-octyne **3** and triethylsilane **2** catalysed by Pt₁ (Table 1, entry 3 in the main text).

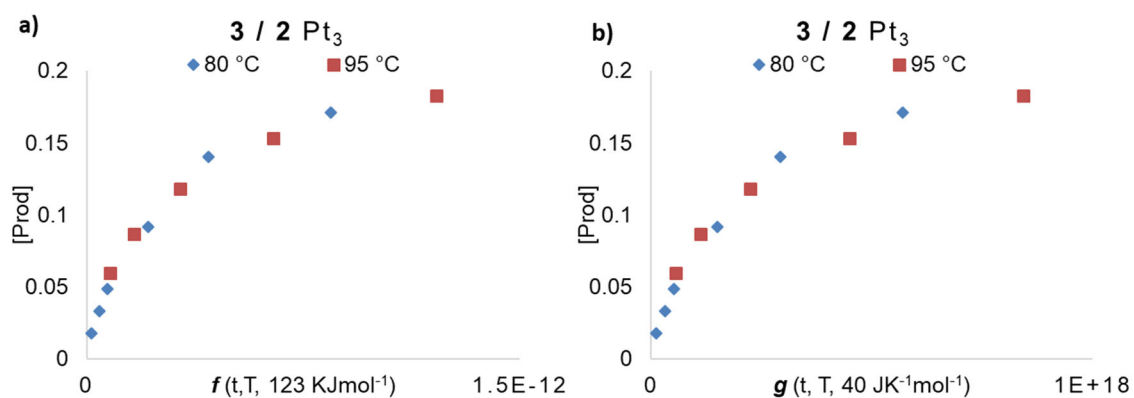


Figure S13. Application of the graphical method to the calculation of transition state enthalpy (a) and entropy (b) of 1-octyne **3** and triethylsilane **2** catalysed by Pt₃ (Table 1, entry 4 in the main text).

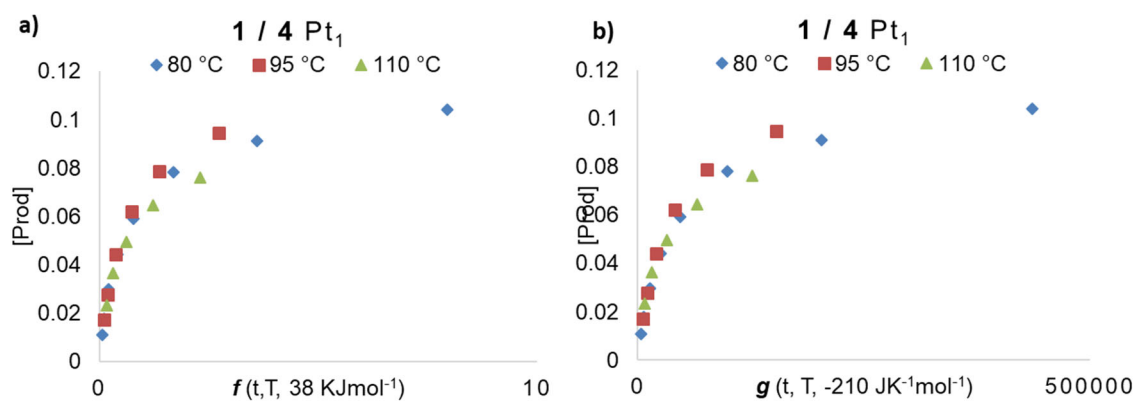


Figure S14. Application of the graphical method to the calculation of transition state enthalpy (a) and entropy (b) of phenylacetylene **1** and 1,1,3,3-tetramethyldisiloxane **4** catalysed by Pt₁ (Table 1, entry 5 in the main text).

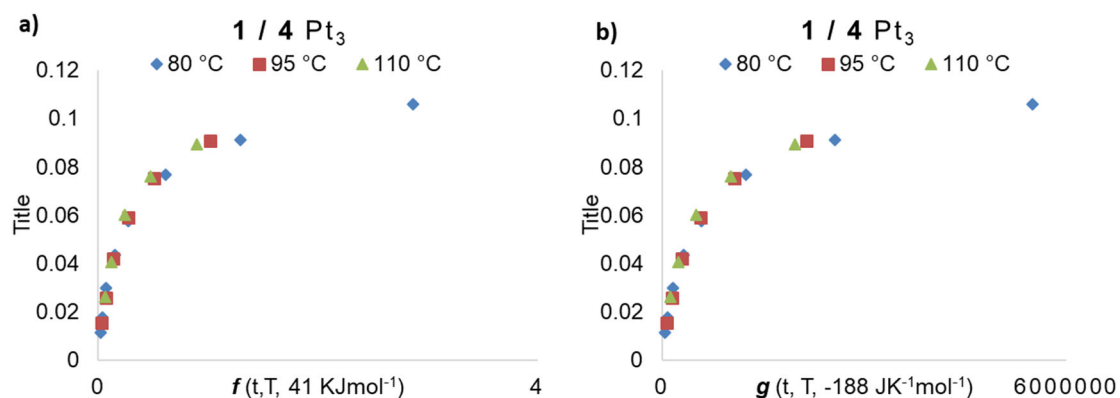


Figure S15. Application of the graphical method to the calculation of transition state enthalpy (a) and entropy (b) of phenylacetylene **1** and 1,1,3,3-tetramethyldisiloxane **4** catalysed by Pt₃ (Table 1, entry 6 in the main text).

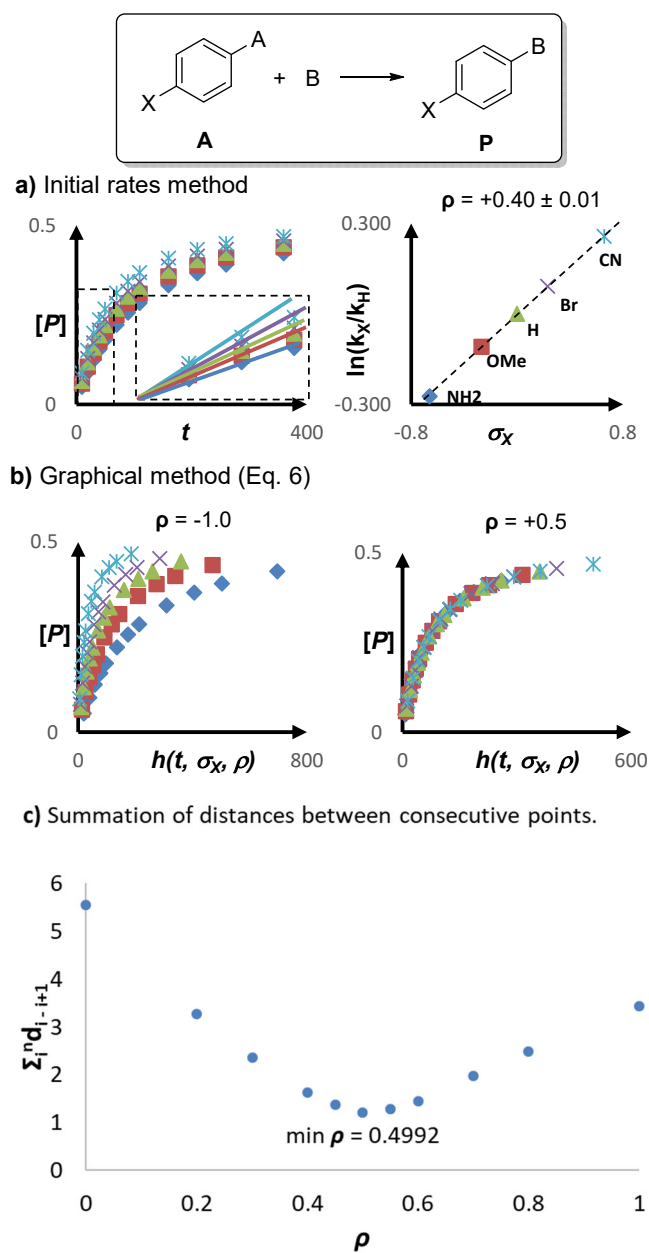
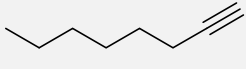
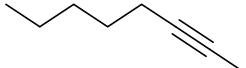
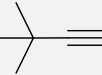
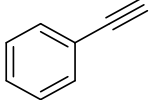
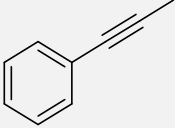
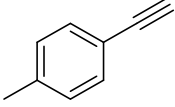
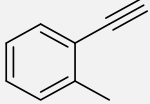
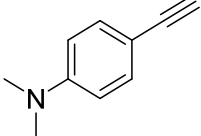
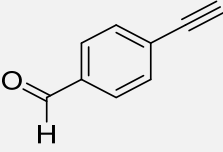
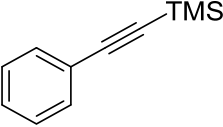
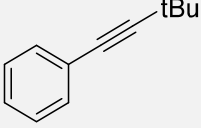
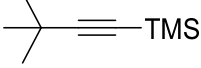


Figure S16. Comparison of a) initial rates method with b) this graphical analysis to calculate Hammett parameter (ρ). A simulated bimolecular reaction was considered in which one of the reagents (A) is a *para*-substituted aromatic ring. c) Summation of the distances between consecutive points for different values of ρ . As can be seen the sum of the distances converge towards the real value of ρ (0.5), reaching the minimum at $\rho = 0.4992$, which constitutes a deviation of 0.1% with respect to the real value.

Hydrosilylation of alkynes. Reactivity, computational and mechanism.

Table S12. Partial charges of the alkyne carbon atoms for different alkynes calculated by Huckel model.

Alkyne	C _{int}	C _{ext}	H	C _{int} -C _{ext}
	0.107	-0.255	0.053	0.362
	-0.063	-0.080	-	0.017
	0.115	-0.276	0.053	0.391
	0.136	-0.306	0.052	0.442
	-0.019	-0.116	-	0.097
	0.136	-0.317	0.052	0.452
	0.139	-0.3155	0.0515	0.455
	0.123	-0.414	0.0515	0.537
	0.133	-0.282	0.0515	0.415
	0.095	-0.470	1.163	0.565
	-0.052	-0.102	-	0.050
	0.062	-0.408	1.164	0.470

	-0.100	-0.054	-	-0.047
--	--------	--------	---	--------

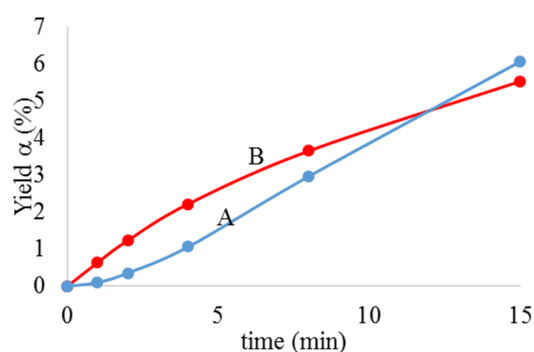


Figure S17. Hydrosilylation of phenylacetylene (0.5 M) with triethylsilane using Pt_1 ($2.5 \cdot 10^{-5}$ M) catalyst without (A) or with silanepyridine (B). Kardstedt's catalyst present an induction time.

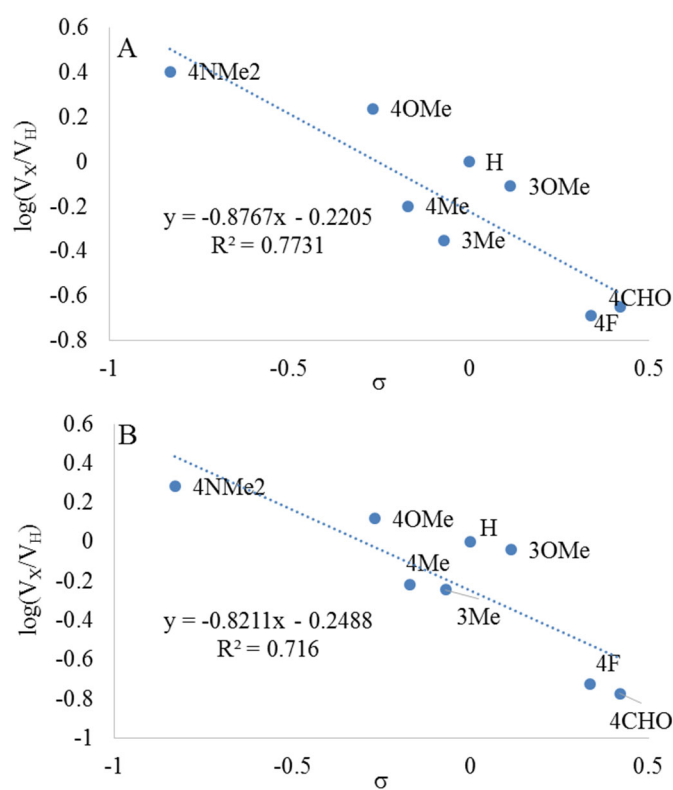


Figure S18. Hammett plots for *para*- and *meta*-substituted ethynylbenzenes. A) α -product, B) β -product. Reaction conditions: alkyne 0.5 mmol, HSiEt_3 0.6 mmol, Pt Kardstedt 0.005 mol%, toluene (1 mL), 110 °C.

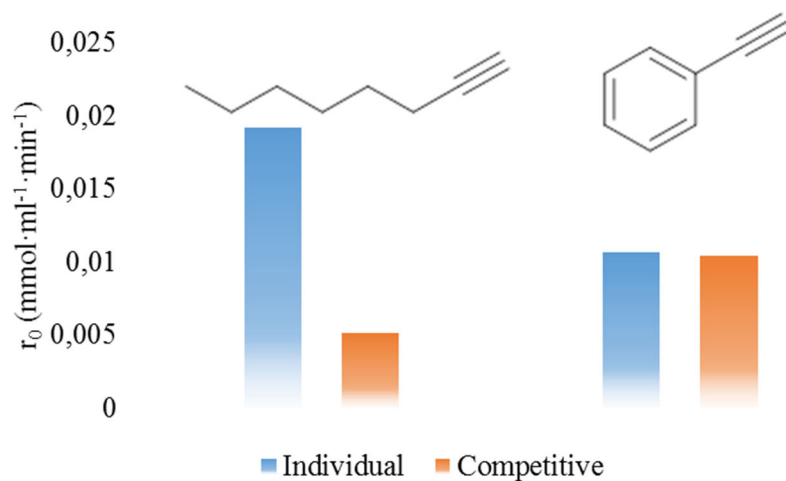


Figure S19. Reaction rate for the hydrosilylation of 1-octyne (left) and phenylacetylene (right) individually and together. Individual experiments conditions: alkyne 0.5 mmol, silane 0.6 mmol, Pt Kardstedt $2.5 \cdot 10^{-5}$ mmol, toluene 1 mL, 110 °C. Competitive experiments: 1-octyne 0.25 mmol, phenylacetylene 0.25 mmol, Pt Kardstedt $2.5 \cdot 10^{-5}$ mmol, toluene 1 mL, 110 °C.

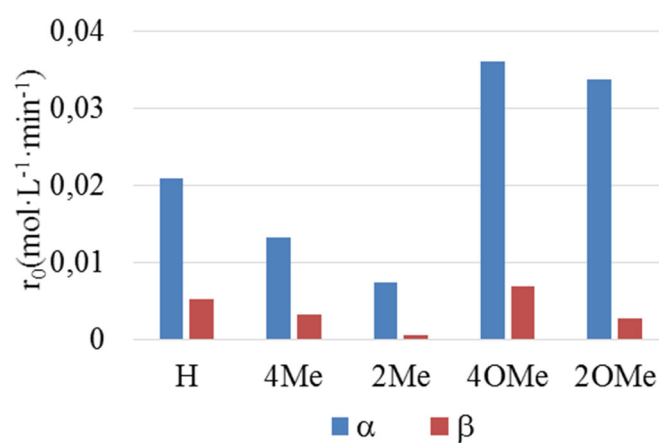


Figure S20. Reaction rate for different substituted phenylacetylenes catalysed by Pt₃

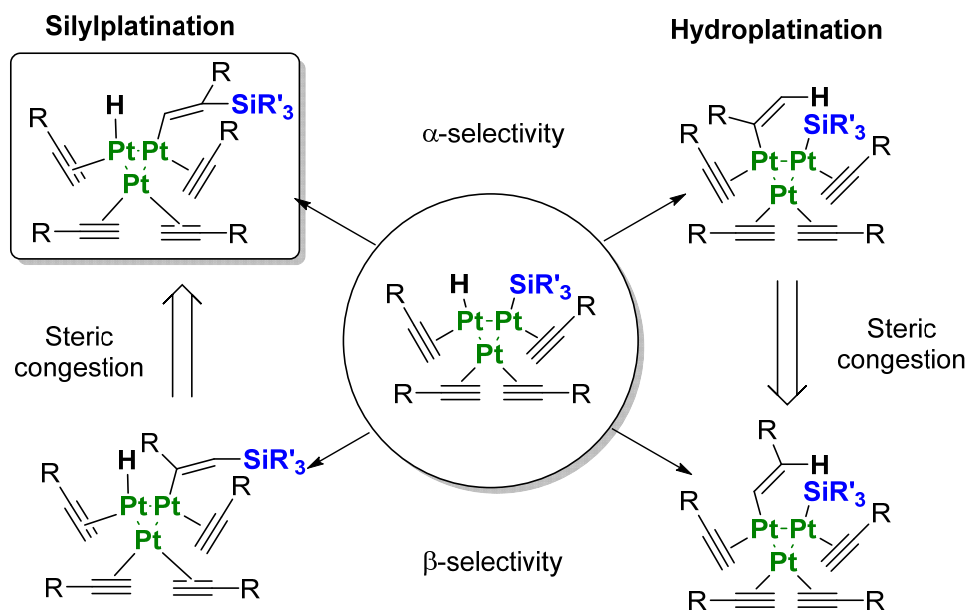


Figure S21. Scheme of different possibilities for migratory insertion through hydro- and silylplatination to yield α and β isomers catalysed by Pt₃ and steric factors affecting each one.

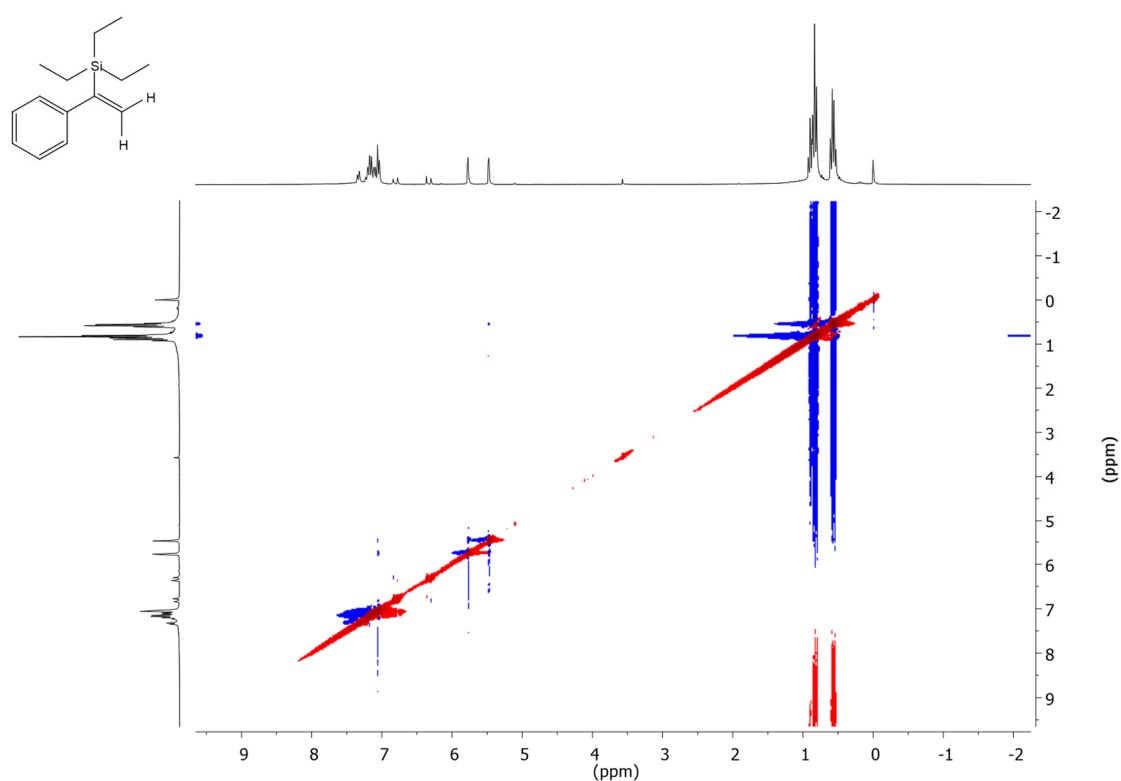


Figure S22. NOESY of the purified product between phenylacetylene 0.5 mmol and HSiEt₃ 0.6 mmol in 1 mL of toluene with Pt Kardstedt (0.005 mol%) at 110 °C.

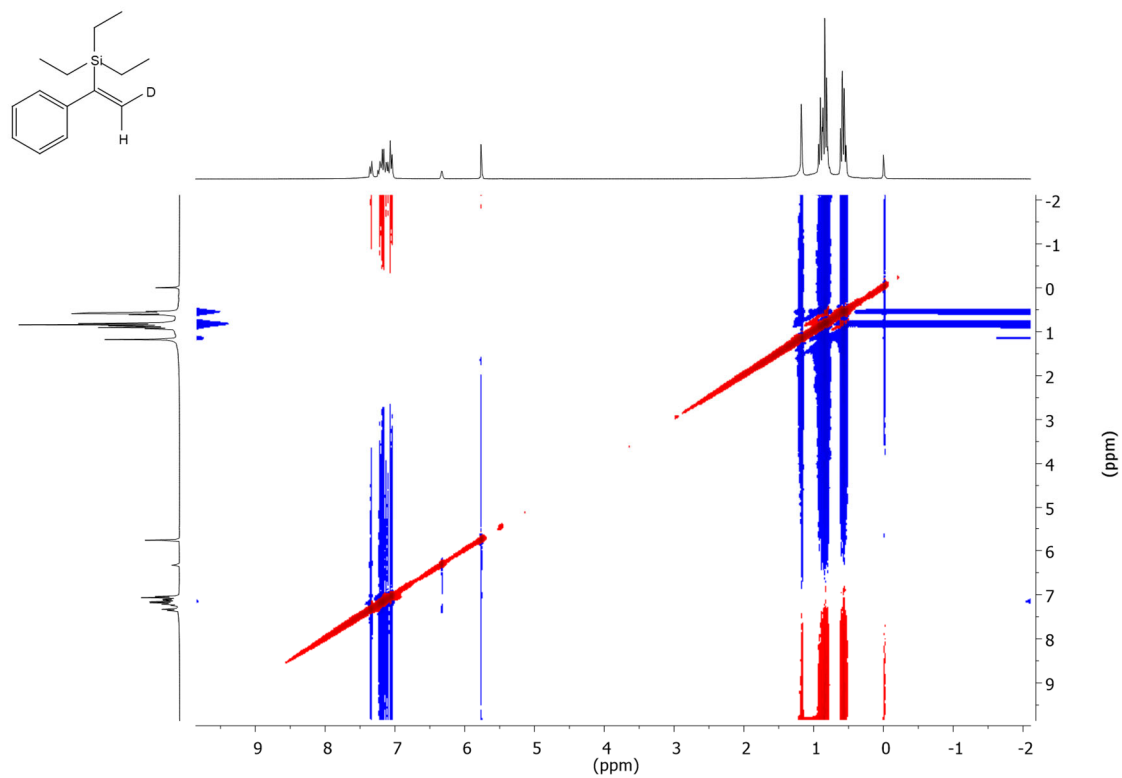


Figure S23. NOESY of the purified product between phenylacetylene 0.5 mmol and DSiEt₃ 0.6 mmol in 1 mL of toluene with Pt Kardstedt (0.005 mol%) at 110 °C.

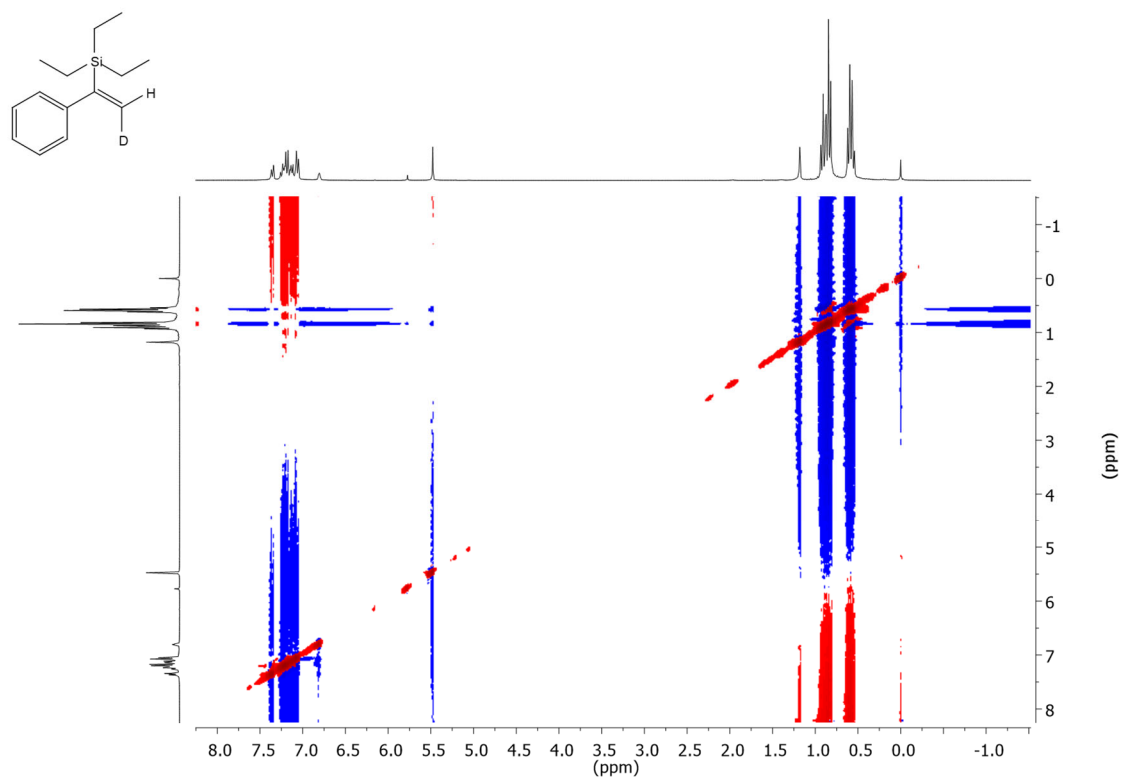


Figure S24. NOESY of the purified product between deuterated phenylacetylene 0.5 mmol and HSiEt₃ 0.6 mmol in 1 mL of toluene with Pt Kardstedt (0.005 mol%) at 110 °C.

$$0 = \frac{d[F]}{dt} = k_4[E][A] - k_5[F][A]^2$$

$$0 = \frac{d[E]}{dt} = k_3[D] - k_4[E][A]$$

$$0 = \frac{d[D]}{dt} = k_2[C][S] - k_{-2}[D][A] - k_3[D]$$

$$0 = \frac{d[C]}{dt} = k_1[B][S] - k_{-1}[C][A] + k_2[C][S] - k_{-2}[D][A]$$

$$0 = \frac{d[B]}{dt} = k_5[F][A]^2 - k_1[B][S] + k_{-1}[C][A]$$

$$[Pt^0] = [B] + [C] + [D] + [E] + [F]$$

These equations were worked out to obtain an equation for the rate of product formation, which is shown below:

$$\frac{d[P]}{dt} = \frac{k_1 k_2 k_3 k_4 k_5}{\{(k_{-1}[A] + k_1[S])(k_{-2}[A] + k_3) + k_2(k_3 k_5 [A]^2 + k_1[S])[S]\} k_4 k_5 [A]^2 + k_1 k_2 k_3 (k_5 [A] + k_4)[S]^2} [S]^2 [A]^2 [Pt^0]$$

Through kinetic measurements, we know that reaction rate always increases with higher silane concentration and decreases with alkyne concentration, at least in the all experiments performed in the study. Therefore, we can omit the $[S]^2$ term in the denominator because is irrelevant in a broad range of reaction conditions. The approximated equation will stay as follows:

$$\frac{d[P]}{dt} = \frac{k_1 k_2 k_3}{(k_{-1}[A] + k_1[S])(k_{-2}[A] + k_3) + k_2(k_3 k_5 [A]^2 + k_1[S])[S]} [S]^2 [Pt^0]$$

Kinetic data measured fits well to the equation after performing the proper modifications and approximations convenient for each case and explains the quadratic dependence of reaction rate [silane] at low concentrations.

Theoretical kinetic equation for Pt₃ and discussion

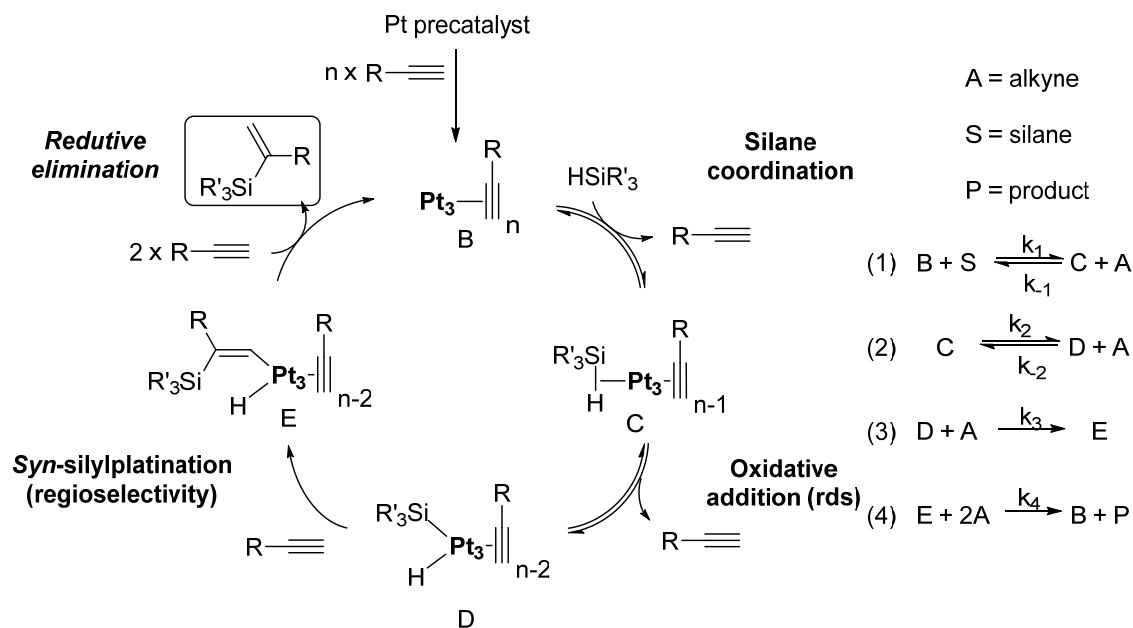


Figure S26. Kinetic equation elucidation from elementary steps of the catalytic cycle for Pt₃ applying steady state approximation.

Steady state approximation was applied to equations 1-2 (intermediates B-E) in order to obtain the rate for every intermediate of the catalytic cycle. Equation 4 was used to obtain the rate of product formation.

$$\text{rate} = \frac{d[P]}{dt} = k_4[E][A]^2$$

$$0 = \frac{d[E]}{dt} = k_3[D][A] - k_4[E][A]^2$$

$$0 = \frac{d[D]}{dt} = k_2[C] - k_{-2}[D][A] - k_3[D][A]$$

$$0 = \frac{d[C]}{dt} = k_1[B][S] + k_{-2}[D][A] - k_{-1}[C][A] - k_2[C]$$

$$0 = \frac{d[B]}{dt} = k_4[E][A]^2 + k_{-1}[C][A] - k_1[B][S]$$

$$[Pt^0] = [B] + [C] + [D] + [E]$$

These equations were worked out to obtain an equation for the rate of product formation which is shown below.

$$\text{rate} = \frac{d[P]}{dt} = \frac{k_1 k_2 k_3 k_4}{\{k_2 k_3 + (k_{-2} + k_3)(k_{-1}[A] + k_1[S])\} k_4 [A]^2 + k_1 k_2 k_4 [A][S] + k_1 k_2 k_3 [S]} [S][A]^2 [Pt^0]$$

Under the diverse conditions tested for the hydrosilylation of phenylacetylene with triethylsilane, experimental rate always increases with higher silane concentration and decreases or remains constant with higher alkyne concentration, showing the high affinity of the platinum for the alkyne. On this basis we can assume $[A]^2$ term is the most relevant in the denominator and excluding the other terms we obtain the following equation:

$$\frac{d[P]}{dt} = \frac{k_1 k_2 k_3}{k_2 k_3 + (k_{-2} + k_3)(k_{-1}[A] + k_1[S])} [S][Pt^0]$$

Which very much resembles the experimental equation obtained with the preliminary kinetic study. Kinetic data measured fits well to the equation after performing the proper modifications and approximations convenient for each case. We have used the same equation for both Pt_1 and Pt_3 species, since the mechanism is similar, according to the experiments that have been carried out. Kinetic constants change for the different platinum species, but also change for different silanes, alkynes and even solvent, since every single step has a characteristic kinetic constant for the reagents.



CH-alpha-H.mov



TS-1-alpha-H.mov

Movie 1. Chalk-Harrod (CH, left) and **TS-1** (right) intermediates for the formation of the alpha-product after hydride insertion.



CH-alpha-Si.mov



TS-1-alpha-Si.mov

Movie 2. Chalk-Harrod (CH, left) and **TS-1** (right) intermediates for the formation of the alpha-product after silylation.



CH-beta-H.mov



TS-1-beta-H.mov

Movie 3. Chalk-Harrod (CH, left) and **TS-1** (right) intermediates for the formation of the beta-product after hydride insertion.



CH-beta-Si.mov



TS-1-beta-Si.mov

Movie 4. Chalk-Harrod (CH, left) and **TS-1** (right) intermediates for the formation of the beta-product after silylation.

Hydrosilylation of alkenes.

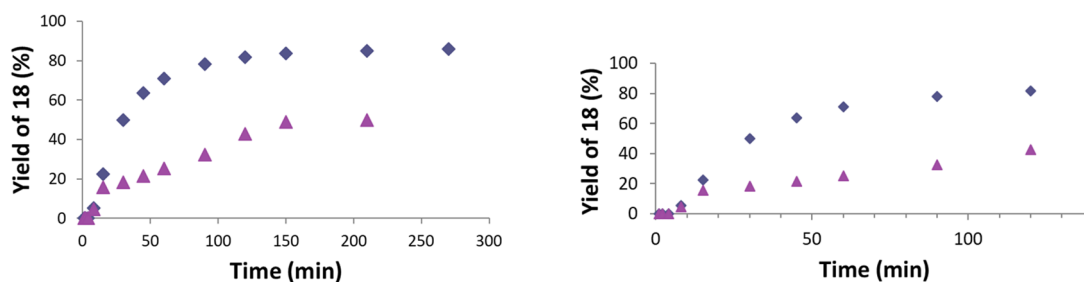


Figure S27. Left: Kinetics for the hydrosilylation of styrene **16** (0.5 M) with dimethylphenylsilane **17** (1.2 equivalents) catalysed by Pt₁/MOF to give (2-phenylethyl)dimethylphenylsilane **18** in toluene at 110 °C (blue diamonds) and after filtering the catalyst in hot at 15 min reaction time (pink triangles). Right: amplification of the points in the first 2 hours.

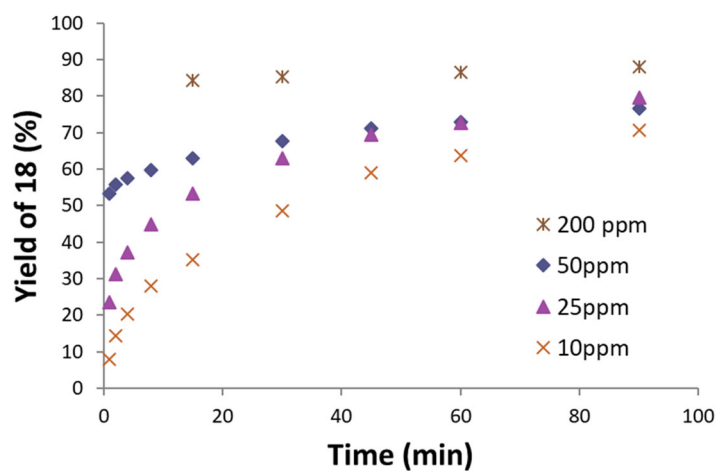


Figure S28. Kinetics for the hydrosilylation of styrene **16** (0.5 M) with dimethylphenylsilane **17** (1.2 equivalents) catalysed by Karstedt's catalyst in toluene at 110 °C.

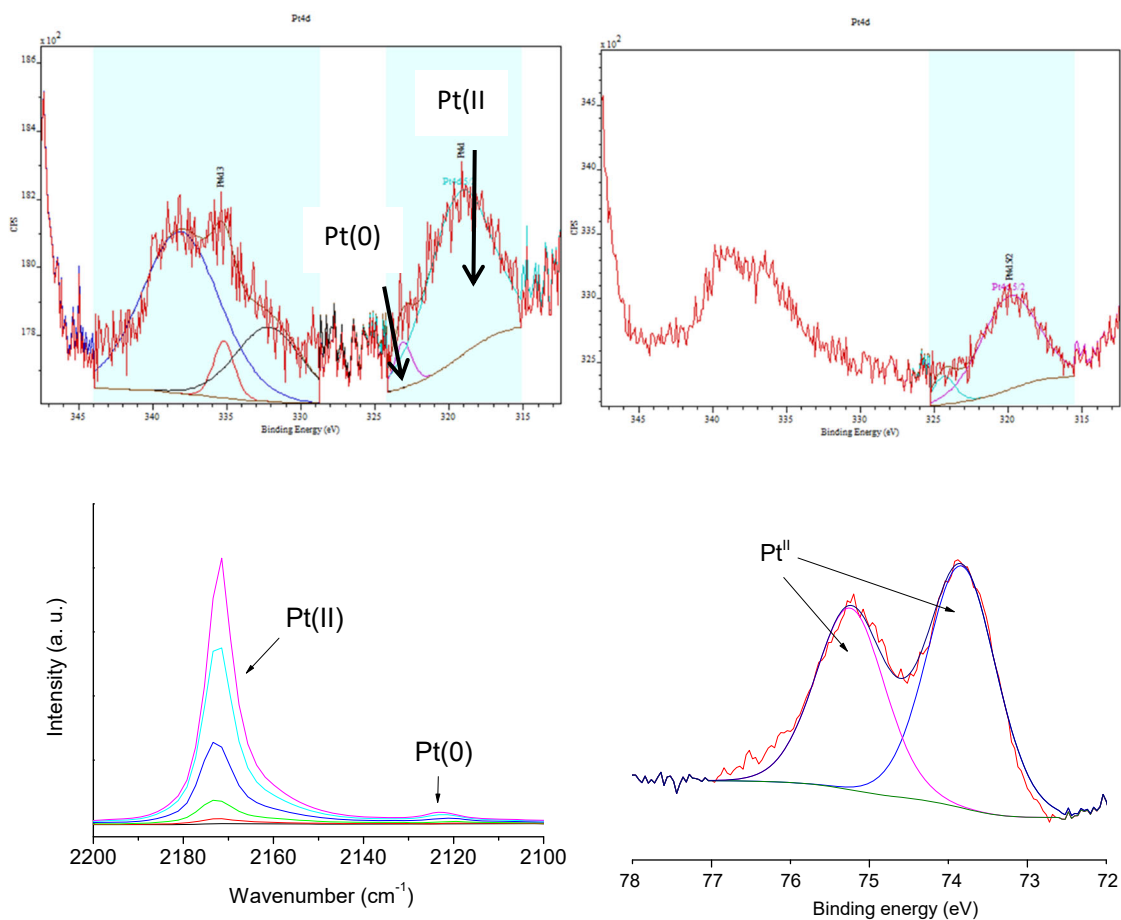
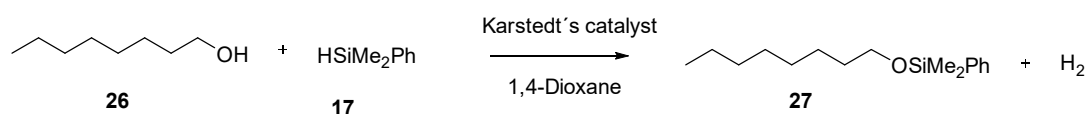


Figure S29. Top: Deconvoluted platinum 4d X-ray photoelectron spectroscopy (XPS) peaks for Pt₁/NaY calcined at 100 °C (left) and 200 °C (right) for 24 h. The Pt(II)/Pt(0) ratio is ca. 20 and 10, respectively. The typical Pt_{4f} peaks were not employed because superimpose with the Al_{2p} peaks of the zeolite. Bottom left: CO-probe low temperature IR measurement of Pt₁/NaY calcined at 200 °C, at increasing CO doses.^{S17} Bottom right: Pt_{4f} XPS of Pt₁/MOF.^{S2}

Dehydrogenative silylation of alcohols.

Table S13. Catalytic results for the hydrosilylation of 1-octanol **26** with dimethylphenylsilane **17** to give octyldimethylphenylsiloxane **27** in 1,4-dioxane solvent with different amounts of Karstedt's catalyst. GC yields using *n*-dodecane as an internal standard. Tests with other solvents gave lower yields.



Entry	mmol 26	mmol 17	Karstedt (ppm)	Solvent volume (ml)	T (°C)	Time (h)	27 (%)	TOF (h ⁻¹)	TON
1	0.25	0.25	100	0.5	100	24	8	33	790
2	0.25	0.25	100	1.0	110	20	5	47	931
3	0.25	0.25	100	0.25	110	20	15	37	733
4	0.25	0.25	100	0.5	110	20	9	45	894
5	0.25	0.25	200	0.5	110	20	16	40	801
6	0.5	0.25	100	0.5	110	20	19	95	1908
7	0.25	0.5	100	0.5	110	20	42	208	4154
8	0.25	0.5	100	0.25	110	19	96	126	2389

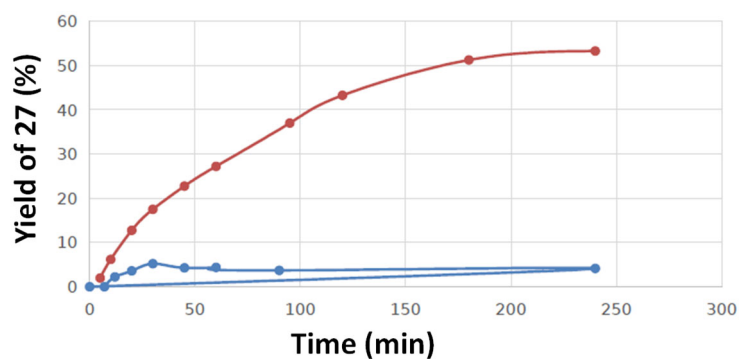


Figure S30. Kinetics for the dehydrogenative hydrosilylation of 1-octanol **26** with dimethylphenylsilane **17** to give octyldimethylphenylsiloxane **27**, with a Pt-supported solid catalyst in 1,4-dioxane at 110 °C, after filtering the solid catalyst in hot at 15 min reaction time (blue points) or not (red points). GC yields using *n*-dodecane as an internal standard.

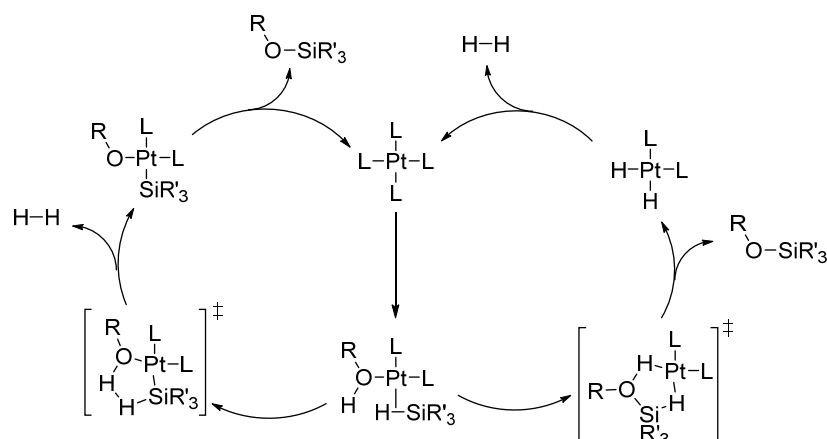


Figure S31. Tentative mechanism for the dehydrogenative silylation of alcohols based on metal(oid) cycles.

References.

- S1 A. I. Serykh, O. P. Tkachenko, V. Y. Borovkov, V. B. Kazansky, M. Beneke, N. I. Jaeger and G. Schulz–Ekloff, *Phys. Chem. Chem. Phys.*, 2000, **2**, 5647–5652.
- S2 M. A. Rivero–Crespo, M. Mon, J. Ferrando–Soria, C. W. Lopes, M. Boronat, A. Leyva–Perez, A. Corma, J. C. Hernandez–Garrido, M. Lopez–Haro, J. J. Calvino, E. V Ramos–Fernandez, D. Armentano and E. Pardo, *Angew. Chem., Int. Ed.*, 2018, **57**, 17094–17099.
- S3 M. A. Rivero–Crespo, A. Leyva–Perez and A. Corma, *Chem. – A Eur. J.*, 2017, **23**, 1702–1708.
- S4 S. Nakamura, M. Uchiyama and T. Ohwada, *J. Am. Chem. Soc.*, 2005, **127**, 13116–13117.
- S5 X. Yang and C. Wang, *Chin. J. Chem.*, 2018, **36**, 1047–1051.
- S6 A. Sanagawa and H. Nagashima, *Organometallics*, 2018, **37**, 2859–2871.
- S7 a) W. Xue, R. Shishido and M. Oestreich, *Angew. Chem., Int. Ed.*, 2018, **57**, 12141–12145, b) X. Yang and C. Wang, *Chin. J. Chem.* 2018, **36**, 1047–1051.
- S8 T. Mitsudome, S. Fujita, M. Sheng, J. Yamasaki, K. Kobayashi, T. Yoshida, Z. Maeno, T. Mizugaki, K. Jitsukawa and K. Kaneda, *Green Chem.*, 2019, **21**, 4566–4570.
- S9 S. Kim, M. S. Kwon and J. Park, *Tetrahedron Lett.*, 2010, **51**, 4573–4575.
- S10 a) J. Bergueiro, J. Montenegro, C. Saa and S. Lopez, *RSC Adv.*, 2014, **4**, 14475–14479; b) L. Süsse, J. H. W. LaFortune, D. W. Stephan and M. Oestreich, *Organometallics* 2019, **38**, 712–721; c) G. Argouarch, *New J. Chem.*, 2019, **43**, 11041–11044.
- S11 J.–D. Chai and M. Head–Gordon, *Phys. Chem. Chem. Phys.*, 2008, **10**, 6615–6620.
- S12 a) J. P. Cerón–Carrasco, J. Ruiz, C. Vicente, C. de Haro, D. Bautista, J. Zúñiga and A. Requena, *J. Chem. Theory Comput.*, 2017, **13**, 3898–3910; b) D. Veclani, A. Melchior, M. Tolazzi and J. P. Cerón–Carrasco, *J. Am. Chem. Soc.*, 2018, **140**, 14024–14027.
- S13 F. Weigend and R. Ahlrichs, *Phys. Chem. Chem. Phys.*, 2005, **7**, 3297–3305.
- S14 a) A. Melchior, E. Sánchez–Marcos, R. Pappalardo and J. M. Martínez, *Theor. Chem. Acc.*, 2011, **128**, 627–638; b) A. Melchior, E. Peralta, M. Valiente, C. Tavagnacco, F. Endrizzi and M. Tolazzi, *Dalt. Trans.*, 2013, **42**, 6074–6082; c) A. Melchior, J. M. Martínez, R. Pappalardo and E. Sánchez–Marcos, *J. Chem. Theory Comput.*, 2013, **9**, 4562–4573.
- S15 J. Tomasi, B. Mennucci and R. Cammi, *Chem. Rev.*, 2005, **105**, 2999–3093.
- S16 Gaussian 16, Revision A.03, M. J. Frisch, G. W. Trucks, H. B. Schlegel, G. E. Scuseria, M. A. Robb, J. R. Cheeseman, G. Scalmani, V. Barone, G. A. Petersson, H. Nakatsuji, X. Li, M. Caricato, A. V. Marenich, J. Bloino, B. G. Janesko, R. Gomperts, B. Mennucci, H. P. Hratchian, J. V. Ortiz, A. F. Izmaylov, J. L. Sonnenberg, D. Williams–Young, F. Ding, F. Lipparini, F. Egidi, J. Goings, B. Peng, A. Petrone, T. Henderson, D. Ranasinghe, V. G. Zakrzewski, J. Gao, N. Rega, G. Zheng, W. Liang, M. Hada, M. Ehara, K. Toyota, R. Fukuda, J. Hasegawa, M. Ishida, T. Nakajima, Y. Honda, O. Kitao, H. Nakai, T. Vreven, K. Throssell, J. A. Montgomery, Jr., J. E. Peralta, F. Ogliaro, M. J. Bearpark, J. J. Heyd, E. N. Brothers, K. N. Kudin, V. N. Staroverov, T. A. Keith, R. Kobayashi, J. Normand, K. Raghavachari, A. P. Rendell, J. C. Burant, S. S. Iyengar, J. Tomasi, M. Cossi, J. M. Millam, M. Klene, C. Adamo, R. Cammi, J. W. Ochterski, R. L. Martin, K. Morokuma, O. Farkas, J. B. Foresman and D. J. Fox, Gaussian, Inc., Wallingford CT, 2016.
- S17 P. Rubio–Marques, M. A. Rivero–Crespo, A. Leyva–Perez, A. Corma, *J. Am. Chem. Soc.*, 2015, **137**, 11832–11837.